

# Anatomy of finite-volume effect on hadronic vacuum polarization contribution to muon $g - 2$

---

**Sakura Itatani<sup>a</sup> Hidenori Fukaya<sup>b</sup> Shoji Hashimoto<sup>c,a</sup>**

<sup>a</sup>*The Graduate University for Advanced Studies, SOKENDAI, Tsukuba, Ibaraki 305-0801, Japan*

<sup>b</sup>*Department of Physics, Graduate School of Science, Osaka University, Toyonaka, Osaka 560-0043, Japan*

<sup>c</sup>*Institute for Particle and Nuclear Studies, High Energy Accelerator Research Organization (KEK), Tsukuba, Ibaraki 305-0801, Japan*

*E-mail:* [itasaku@post.kek.jp](mailto:itasaku@post.kek.jp)

**ABSTRACT:** Low-energy spectrum relevant to the lattice calculation of hadronic vacuum polarization contribution to muon anomalous magnetic moment  $a_\mu$  is dominantly given by two-pion states satisfying Lüscher’s finite-volume quantization condition. Finite-volume effects from those states may exhibit power-law dependence on the volume, contrary to an exponential suppression as suggested by chiral effective theory. Employing the finite-volume state decomposition of Euclidean correlators, we systematically investigate the volume dependence. Phenomenological inputs are used for  $\pi\pi$  phase shift and time-like pion form factor. Our estimate for the finite-volume effects on  $a_\mu$  is larger than previous works and has a different volume scaling. Numerical results are given for the “window” observables of  $a_\mu$ .

---

## Contents

<b>1</b>	<b>Introduction</b>	<b>1</b>
<b>2</b>	<b>Two-pion contribution to <math>a_\mu^{\text{HVP,LO}}</math></b>	<b>3</b>
<b>3</b>	<b>Two-pion contribution in the non-interacting case</b>	<b>5</b>
3.1	Current correlator	5
3.2	Contribution $a_\mu^{\text{HVP,LO}}$	8
<b>4</b>	<b>Two-pion contribution in the interacting case</b>	<b>11</b>
4.1	Finite-volume energy spectrum	11
4.2	Matrix element from Gounaris-Sakurai model	13
4.3	Sum over the low-lying $\pi\pi$ states	15
4.4	Results for $a_\mu^{\text{HVP,LO}}$	18
<b>5</b>	<b>Finite volume effects for <math>a_\mu^{\text{HVP,LO}}</math></b>	<b>19</b>
5.1	Total, and sharply cut time windows	19
5.2	Smeared time windows	23
<b>6</b>	<b>Conclusion</b>	<b>24</b>

---

## 1 Introduction

The finite-volume effect is one of the most important sources of systematic error in the lattice QCD computation of hadronic vacuum polarization (HVP) contribution to muon anomalous magnetic moment  $a_\mu = (g_\mu - 2)/2$ . In particular, the isovector component at the leading order, written as  $a_\mu^{\text{HVP,LO}}$ , gives the largest contribution and thus potentially involves the most significant systematic errors. For example, in the BMW calculation in 2020 [1] the finite-volume effect at their reference lattice of size  $L_{\text{ref}} \simeq 6.3$  fm is estimated as  $19(3) \times 10^{-10}$ , which is much larger than the error of the current experimental average,  $\sim 2 \times 10^{-10}$  [2]. Given the limitation of the lattice volume one can simulate with currently available computational resources, a reliable estimate of the finite-volume effect is of great relevance to the test of the Standard Model through  $a_\mu$ . In fact, an estimated finite-volume correction is added to the result to obtain the final result in [1], and its uncertainty is estimated to be approximately the same size as the experimental error.

Some theoretical estimates of the correction due to the finite spatial and temporal extent of the lattice are available from chiral perturbation theory (ChPT) [3–6] or from more general approaches [7, 8], and a correction that is suppressed at least as  $\exp(-m_\pi L)$  is found in the leading order, for the pion mass  $m_\pi$  and spatial extent of the lattice  $L$ . There is, on the other hand, an argument that suggests a dependence of power law at least

from the region of large Euclidean time separation of the current correlator that enters in the evaluation of HVP [7, 8]. This is understood as follows. In a finite spatial volume, the energy levels are quantized according to Lüscher’s condition [9] and their level spacing scales as an inverse power of  $L$ . A sum of the contributions from these quantized states could naturally develop a power-law dependence like  $1/L^\alpha$ , especially from the lowest end of the spectrum. This effect could become most important for large Euclidean time separations where only a few lowest energy levels dominate, and is relevant for the estimate of  $a_\mu^{\text{HVP,LO}}$ , as it receives a significant contribution from the time separation of the order of the inverse muon mass  $1/m_\mu \sim 2$  fm. The transition of such power-law dependence to the exponential one as expected from other analyses and its numerical impact are still to be understood.

In this work, we systematically study the effect of finite volume on  $a_\mu^{\text{HVP,LO}}$  using the framework to construct finite-volume Euclidean correlation functions from the phenomenological input. The two-pion states in a finite volume are identified using Lüscher’s formula [9], and their transition matrix element from the vacuum is given using the Lellouch-Lüscher factor [10, 11] as explicitly formulated in [12]. In a finite box, the rotational symmetry is violated and different angular momentum states can mix. In the present case of the angular momentum  $J = 1$   $\pi\pi$  states, the states of  $J = 3$  can mix, for example. We neglect such effects, assuming that their effect on the estimate of the finite-volume effect is not significant.

An estimate of  $a_\mu^{\text{HVP,LO}}(L)$  at a finite volume  $L$  is then obtained using the time-momentum representation [13] from the Euclidean correlation functions. Phenomenological inputs are needed for the two-pion scattering phase shift  $\delta_1^1(k)$  (for isospin  $I = 1$  and angular momentum  $J = 1$ ) and for the time-like pion form factor  $F_\pi(s)$ . In our analysis, we use the commonly adopted Gounaris-Sakurai model [14]. We also assume that inelastic state contributions, such as those from four pions and other higher-energy states, can be neglected when estimating the finite-volume effect. This framework has been applied in [1, 11, 15–19] to estimate the finite-volume effect; our work extends the framework to include essentially all energy  $\pi\pi$  eigenstates (see Section 4.3 for details), while most of the previous works treated only a small number of lowest states so that the volume analyzed is limited or other methods have to be combined in the analysis.

Contributions from different length scales are commonly studied using the “window” quantities [20], as described in the community white paper [21]. Three length scales are considered: short-distance window (SD), intermediate window (W), and long-distance window (LD). Their region of Euclidean time integral in the time-momentum representation is defined by  $[0, 0.4]$  fm,  $[0.4, 1.0]$  fm, and  $[1.0, \infty]$  fm, respectively, allowing a transition region of width 0.15 fm implemented with a sigmoid function. (Details are discussed in Section 5.2.) So far, the simulation results from various groups have been confirmed to agree in the intermediate window (see [22], for example, for a summary of the results from [6, 18, 19, 23–25]). The intermediate window is designed such that the discretization effect and the finite-volume effect are less important. Similar comparison of lattice data in the long-distance window is still missing (but a result of the RBC/UKQCD collaboration appeared recently [26]), and the subject of this work is the finite-volume effect that is expected to become most significant in this window.

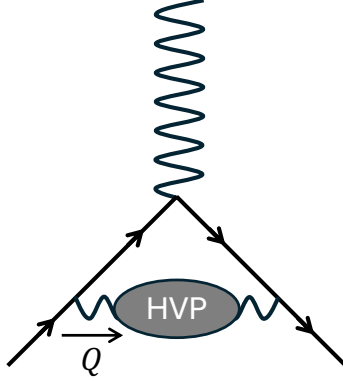


**Figure 1.** Leading-order hadronic vacuum polarization contribution to muon  $g - 2$

The dominant contribution in the long-distance region arises from the two-pion states, for which the interaction vanishes in the low-energy limit. The long-distance physics is therefore expected to be well described by a non-interacting pion states as the zeroth order approximation. The two-pion contribution can be written analytically in that limit (for large Euclidean time separation), and it provides a reference for extrapolation towards the infinite-volume limit. This analysis is described in Section 3.

However, for more realistic estimates of the finite-volume effect, the resonance enhancement of the  $\gamma\pi^+\pi^-$  vertex due to the  $\rho$  meson in the time-like pion form factor plays an important role. Such effect could not be fully incorporated within the framework of ChPT, and the method as used in this work is needed.

We focus on the leading finite-volume effects on the isovector channel, while contributions from other flavours or from isospin breaking are ignored. Finite-volume effects for these states are expected to be much smaller as the mass of involved states is larger.

The structure of this paper is as follows. Section 2 summarizes the standard formulae in the lattice calculation of  $a_\mu^{\text{HVP,LO}}$ . Then, in Section 3 we outline the analytic calculation applicable for non-interacting pions. The analysis is extended to the interacting case in Section 4, and the results for the finite-volume effects for  $a_\mu^{\text{HVP,LO}}$  including the predictions for the window quantities are presented in Section 5. Conclusions with some discussions are stated in Section 6.

## 2 Two-pion contribution to $a_\mu^{\text{HVP,LO}}$

In this section, we summarize the necessary formulae for the evaluation of  $a_\mu^{\text{HVP,LO}}$  to define the notations.

The leading-order (the order of  $\alpha^2$  of fine structure constant  $\alpha$ ) hadronic vacuum polarization contribution to muon anomalous magnetic moment,  $a_\mu^{\text{HVP,LO}}$ , is written as an integral of the vacuum polarization function  $\Pi(Q^2)$  over space-like momentum squared  $Q^2$ :

$$a_\mu^{\text{HVP,LO}} = 4\alpha^2 \int_0^\infty dQ^2 K_E(Q^2) [\Pi(Q^2) - \Pi(0)] \quad (2.1)$$

with a known kernel function  $K(Q^2)$  [27] obtained from an integral of the vertex function in Figure 1. It is given as

$$K_E(Q^2) = \frac{1}{m_\mu^2} \hat{Q}^2 \cdot Z(\hat{Q}^2)^3 \frac{1 - \hat{Q}^2 Z(\hat{Q}^2)}{1 + \hat{Q}^2 Z(\hat{Q}^2)^2} \quad (2.2)$$

with

$$Z(\hat{Q}^2) = -\frac{\hat{Q}^2 - \sqrt{\hat{Q}^4 + 4\hat{Q}^2}}{2\hat{Q}^2}, \quad \hat{Q}^2 \equiv \frac{Q^2}{m_\mu^2} \quad (2.3)$$

for the muon mass  $m_\mu$ . The space-like momentum kernel function  $K_E(Q^2)$  behaves as  $1/(\hat{Q}^2)^3$  for large  $\hat{Q}^2$ , so the contribution from the large energy region is highly suppressed.

The vacuum polarization function  $\Pi(Q^2)$  is defined through

$$(Q_\mu Q_\nu - Q^2 \delta_{\mu\nu}) \Pi(Q^2) = \int d^4x e^{iQx} \langle 0 | j_\mu^{\text{em}}(x) j_\nu^{\text{em}}(0) | 0 \rangle \quad (2.4)$$

with electromagnetic current  $j_\mu^{\text{em}}(x)$ . By a Fourier transform in the time direction, the representation (2.1) can be rewritten in the form of an integral over Euclidean time [13], which is more convenient for lattice QCD calculations:

$$a_\mu^{\text{HVP,LO}} = 4\alpha^2 m_\mu \int_0^{\tau_c} d\tau \tau^3 G(\tau) \tilde{K}_E(\tau). \quad (2.5)$$

An Euclidean correlator  $G(\tau)$  is also obtained by a Fourier transform as

$$G(\tau) \equiv \int d\mathbf{x} \langle 0 | j_z^{\text{em}}(\tau, \mathbf{x}) j_z^{\text{em}}(0) | 0 \rangle, \quad (2.6)$$

where we take the electromagnetic currents  $j_\mu^{\text{em}}(\tau, \mathbf{x})$  in a spatial direction  $\mu = z$ . It is projected to zero spatial momentum, and separated in Euclidean time  $\tau$ . When obtained in a finite volume, we denote the correlator by  $G(\tau, L)$ , and the corresponding  $a_\mu^{\text{HVP,LO}}$  obtained through (2.5) as  $a_\mu^{\text{HVP,LO}}(L)$ . The kernel function  $\tilde{K}_E(\tau)$  is written in terms of the corresponding Euclidean momentum-space representation  $K_E(\omega^2)$  (2.2) as [27]

$$\tilde{K}_E(\tau) \equiv \frac{2}{m_\mu \tau^3} \int_0^\infty \frac{d\omega}{\omega} K_E(\omega^2) \left[ \omega^2 \tau^2 - 4 \sin^2 \frac{\omega \tau}{2} \right]. \quad (2.7)$$

The upper limit  $\tau_c$  of the integral (2.5) should be set to infinity, but in practical lattice calculations the integral is cut off at a certain value of  $\tau_c$ . As shown in Figure 2, the integrand peaks around  $\tau = 1$  fm and rapidly decays towards larger  $\tau$ . The contributions from the time intervals [0,1] fm, [1,2] fm, [2,5] fm are about 34%, 39%, 27%, respectively, and that from the region beyond 5 fm is below 1%. The long-distance (LD) region beyond 1 fm (with a smearing of 0.15 fm as discussed above) [21] roughly accounts for 60% of the total  $a_\mu^{\text{HVP,LO}}$ .

In the long-distance region the Euclidean correlator is dominated by two-pion states and written as

$$G(\tau, L) = \sum_n |\langle 0 | j_z^{\text{em}} | \pi\pi, n \rangle_V|^2 e^{-E_{\pi\pi, n} \tau} \quad (2.8)$$

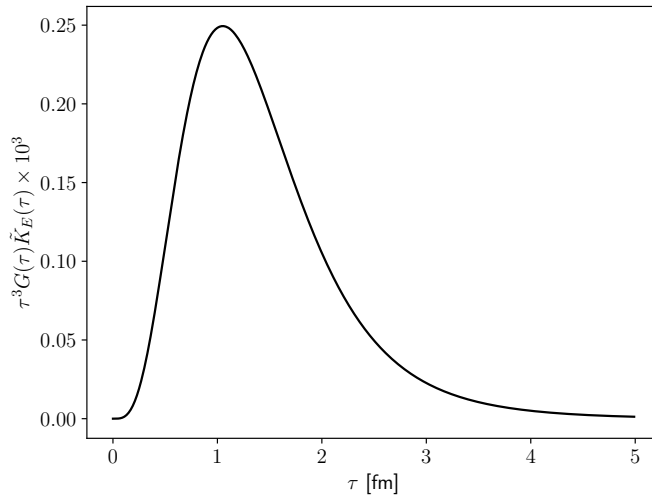


**Figure 2.** Integrand of the time momentum representation (2.5). The Gounaris-Sakurai model for the time-like pion form factor is used as described in the following sections.

in a finite volume  $V = L^3$ . Here, the isovector channel is assumed and an isospin index for the two-pion state  $|\pi\pi, n\rangle_V$  is suppressed. The states are discretized in a finite volume, and the energy of  $n$ -th state  $|\pi\pi, n\rangle_V$  is denoted as  $E_{\pi\pi, n}$ .

In the infinite volume limit, where the two-pion states are simply labeled by the momenta  $\mathbf{k}$  and  $\mathbf{k}'$  of the pions in the asymptotic state, the matrix elements in (2.8) are expressed in terms of the pion form factor  $F_\pi(s)$ :

$$\langle 0 | j_\mu | \pi_{\mathbf{k}} \pi_{\mathbf{k}'}; \text{in} \rangle = - \langle \pi_{\mathbf{k}} \pi_{\mathbf{k}'}; \text{out} | j_\mu | 0 \rangle = e^{i\delta_1^1(\mathbf{k}-\mathbf{k}')} (\mathbf{k} - \mathbf{k}')_\mu F_\pi(s). \quad (2.9)$$

Here we consider the case of the center-of-mass frame  $\mathbf{k} + \mathbf{k}' = 0$ . The momentum transfer is then  $s = 4(m_\pi^2 + \mathbf{k}^2)$ . The phase shift of the scattering is denoted as  $\delta_1^1(\mathbf{k} - \mathbf{k}')$ .

We describe the method to construct the finite-volume correlation function  $G(\tau, L)$  from phenomenological inputs for  $F_\pi(s)$  and  $\delta_1^1(\mathbf{k})$  in Section 4.

### 3 Two-pion contribution in the non-interacting case

Before analyzing more realistic cases including interactions between pions, we consider the case of non-interacting pions, in order to gain some idea about possible asymptotic functional forms of the Euclidean correlator and  $a_\mu^{\text{HVP, LO}}(L)$ . It should provide a reasonable approximation at low energy, which is most relevant to the finite-volume effect because the pion interaction vanishes in the (massless and) low-energy limit.

#### 3.1 Current correlator

For non-interacting pions, the two-pion states in (2.8) are identified by their relative momentum  $\mathbf{k}$ . The pion form factor in (2.9) is  $|F_\pi(s)| = 1$  and the phase shift is  $\delta_1^1 = 0$ . For a finite volume  $V = L^3$ , the Euclidean time correlation function is written as (see Appendix

A.3 of [15] as well as Section 2.2.3 of [8])

$$G(\tau, L) = \frac{1}{L^3} \sum_{\mathbf{k}} \frac{k_z^2 e^{-2\sqrt{\mathbf{k}^2 + m_\pi^2} \tau}}{\mathbf{k}^2 + m_\pi^2}, \quad (3.1)$$

where the sum is taken over  $k_i = 2\pi l_i/L$  with integers  $l_i$ . In order for a numerical evaluation, this expression is useful when  $\tau/L \gg 1$  where the summation over  $\mathbf{k}$  converges quickly. When  $\tau/L \sim 1$  or smaller, the following expression is more adequate for numerical evaluation.

Using the Poisson resummation formula for an arbitrary function  $f(p)$

$$\sum_l f\left(\frac{2\pi l}{L}\right) = \int dp \sum_l \delta\left(p - \frac{2\pi l}{L}\right) f(p) = L \sum_n \int \frac{dp}{2\pi} f(p) e^{in p L}, \quad (3.2)$$

we obtain

$$G(\tau, L) = \sum_{\mathbf{n}} \int \frac{d^3 p}{(2\pi)^3} \frac{p_z^2 e^{-2\sqrt{\mathbf{p}^2 + m_\pi^2} \tau}}{\mathbf{p}^2 + m_\pi^2} e^{i\mathbf{n} \cdot \mathbf{p} L}, \quad (3.3)$$

where three-component vector  $\mathbf{n} = (n_x, n_y, n_z)$  consists of integers. Invariance under  $90^\circ$  rotations allows us to replace  $p_z^2$  by  $\mathbf{p}^2/3$ , and using an integral over angular components of  $\mathbf{p}$ , which we denote by  $\theta_p$  and  $\varphi_p$ ,

$$\int_0^{2\pi} d\varphi_p \int_0^\pi d\theta_p \sin \theta_p e^{i|\mathbf{n}|pL \cos \theta_p} = \frac{4\pi \sin(|\mathbf{n}|pL)}{|\mathbf{n}|pL}, \quad (3.4)$$

we have

$$G(\tau, L) = \frac{m_\pi^3}{6\pi^2} \sum_{\mathbf{n}} \int_0^\infty dy \frac{y^4}{y^2 + 1} \frac{\sin(m_\pi L |\mathbf{n}| y)}{m_\pi L |\mathbf{n}| y} e^{-2m_\pi \tau \sqrt{y^2 + 1}}, \quad (3.5)$$

where we have changed a variable as  $p(\equiv |\mathbf{p}|) = y m_\pi$ . Note that the  $\mathbf{n} = \mathbf{0}$  part corresponds to the infinite-volume limit  $L = \infty$ . The non-zero  $|\mathbf{n}|$  terms corresponds to the effect of pion wrapping around the finite-volume lattice. In practice, the sum over  $|\mathbf{n}|$  is truncated.

The effect of pion form factor, or the  $\gamma\pi^+\pi^-$  vertex form factor, may be included by multiplying  $|F_\pi(4(m_\pi^2 + \mathbf{k}^2))|^2$  to the sum over  $\mathbf{k}$  in (3.1). This amounts to inserting  $|F_\pi(4m_\pi^2(1 + y^2))|^2$  in (3.5). However, this may cause a problem when  $|F_\pi(s)|^2$  is a rapidly changing function, as in the case for the  $\rho$ -meson resonance. Since the integrand in (3.5) contains a highly oscillating term  $\sin(m_\pi L |\mathbf{n}| y)$ , the integral could vary drastically for different  $|\mathbf{n}|$  unless  $|\mathbf{n}|$  is large enough to cancel out the oscillation. The condition corresponds to  $|\mathbf{n}| \gg 2\pi/\Delta k_\rho L$ , where  $\Delta k_\rho$  represents the momentum range in which the form factor varies rapidly. For the physical  $\rho$ -meson resonance,  $\Delta k_\rho$  is roughly  $m_\rho \Gamma/8k_\rho \sim 40$  MeV. (Here,  $\rho$  meson mass  $m_\rho = 770$  MeV and width  $\Gamma = 150$  MeV as well as the corresponding pion momentum  $k_\rho = \sqrt{m_\rho^2/4 - m_\pi^2} = 360$  MeV are introduced.) For example, when  $L = 6$  fm the condition implies  $|\mathbf{n}| \gg 5$ . Thus, many terms have to be kept in the wrap-around expansion to introduce the resonance-like pion form factor.

Now we consider the finite-volume correction  $\Delta G(\tau, L) \equiv G(\tau, L) - G(\tau, \infty)$ :

$$\Delta G(\tau, L) = \frac{m_\pi^3}{12\pi^2} \sum_{\mathbf{n} \neq \mathbf{0}} \int_{-\infty}^\infty dy \frac{y^3}{y^2 + 1} \frac{e^{iy m_\pi L |\mathbf{n}|} e^{-2m_\pi \tau \sqrt{y^2 + 1}}}{2im_\pi L |\mathbf{n}|} + \text{c.c.} \quad (3.6)$$

When  $m_\pi\tau \gg 1$ , the small  $y^2$  region dominates the integral, and

$$\begin{aligned}
& \int_{-\infty}^{\infty} dy \frac{y^3}{y^2+1} \frac{e^{iym_\pi L|\mathbf{n}|}}{2im_\pi L|\mathbf{n}|} \exp \left[ -2m_\pi\tau \sqrt{y^2+1} \right] \\
& \sim \int_{-\infty}^{\infty} dy \frac{y^3}{2im_\pi L|\mathbf{n}|} \exp \left[ -2m_\pi\tau (1+y^2/2) + iym_\pi L|\mathbf{n}| \right] \\
& = \frac{e^{-2m_\pi\tau - \frac{m_\pi L^2 \mathbf{n}^2}{4\tau}}}{2im_\pi L|\mathbf{n}|} \int_{-\infty}^{\infty} dy y^3 \exp \left[ -m_\pi\tau \left( y - \frac{iL|\mathbf{n}|}{2\tau} \right)^2 \right] \\
& = \frac{e^{-2m_\pi\tau - \frac{m_\pi L^2 \mathbf{n}^2}{4\tau}}}{2im_\pi L|\mathbf{n}|} \int_{-\infty}^{\infty} dz \left( z + \frac{iL|\mathbf{n}|}{2\tau} \right)^3 \exp \left[ -m_\pi\tau z^2 \right],
\end{aligned} \tag{3.7}$$

where the  $y$  integral is analytically continued to the complex plane and replaced by that of  $z \equiv y - \frac{iL|\mathbf{n}|}{2\tau}$ . Dropping odd functions in  $z$ , we obtain

$$\begin{aligned}
\Delta G(\tau, L) &= \frac{2m_\pi^3}{12\pi^2} \sum_{\mathbf{n} \neq \mathbf{0}} \frac{e^{-2m_\pi\tau - \frac{m_\pi L^2 \mathbf{n}^2}{4\tau}}}{4m_\pi\tau} \int_{-\infty}^{\infty} dz \left( 3z^2 - \frac{L^2|\mathbf{n}|^2}{4\tau^2} \right) \exp \left[ -m_\pi\tau z^2 \right] \\
&= \frac{m_\pi^3}{6\pi^2} \sum_{\mathbf{n} \neq \mathbf{0}} \frac{e^{-2m_\pi\tau - \frac{m_\pi L^2 \mathbf{n}^2}{4\tau}}}{4m_\pi\tau} \left( -\frac{3}{\tau} \frac{\partial}{\partial m_\pi} - \frac{L^2|\mathbf{n}|^2}{4\tau^2} \right) \int_{-\infty}^{\infty} dz \exp \left[ -m_\pi\tau z^2 \right] \\
&= \frac{m_\pi^3}{6\pi^2} \sum_{\mathbf{n} \neq \mathbf{0}} \frac{e^{-2m_\pi\tau - \frac{m_\pi L^2 \mathbf{n}^2}{4\tau}}}{4m_\pi\tau} \left( -\frac{3}{\tau} \frac{\partial}{\partial m_\pi} - \frac{L^2|\mathbf{n}|^2}{4\tau^2} \right) \sqrt{\frac{\pi}{m_\pi\tau}} \\
&= \sqrt{\frac{m_\pi}{\pi^3\tau^5}} \frac{e^{-2m_\pi\tau}}{48} \sum_{\mathbf{n} \neq \mathbf{0}} \left( 3 - \frac{m_\pi L^2|\mathbf{n}|^2}{2\tau} \right) \exp \left( -\frac{m_\pi L^2 \mathbf{n}^2}{4\tau} \right),
\end{aligned} \tag{3.8}$$

which is Eq. (A15) of [15]. Here, using

$$\sum_{\mathbf{n} \neq \mathbf{0}} \left( 3 - \frac{m_\pi L^2|\mathbf{n}|^2}{2\tau} \right) \exp \left( -\frac{m_\pi L^2 \mathbf{n}^2}{4\tau} \right) = \left( 3 + 2m_\pi \frac{\partial}{\partial m_\pi} \right) \sum_{\mathbf{n} \neq \mathbf{0}} \exp \left( -\frac{m_\pi L^2 \mathbf{n}^2}{4\tau} \right)$$

and a formula of the elliptic theta function

$$\vartheta_3(0, q) = 2 \sum_{n=1}^{\infty} q^{n^2} + 1 = \sum_{n=-\infty}^{\infty} q^{n^2},$$

we obtain a compact expression:

$$\Delta G(\tau, L) = \sqrt{\frac{m_\pi}{\pi^3\tau^5}} \frac{e^{-2m_\pi\tau}}{48} \left( 3 + 2m_\pi \frac{\partial}{\partial m_\pi} \right) \left[ \left( \vartheta_3(0, e^{-\frac{m_\pi L^2}{4\tau}}) \right)^3 - 1 \right]. \tag{3.9}$$

For small  $\zeta \equiv e^{-m_\pi L^2/4\tau}$  the elliptic theta function scales as  $\vartheta_3(0, \zeta) \rightarrow 1 + 2\zeta + \dots$ , so that  $\Delta G(\tau, L)$  approaches zero as  $\exp(-m_\pi L^2/4\tau)$ . When  $L \sim 4\tau$ , this is consistent with the well-known estimate of the finite-volume scaling as  $\exp(-m_\pi L)$ . However, we find differences in the shorter and longer distances. In the region of large time separation,



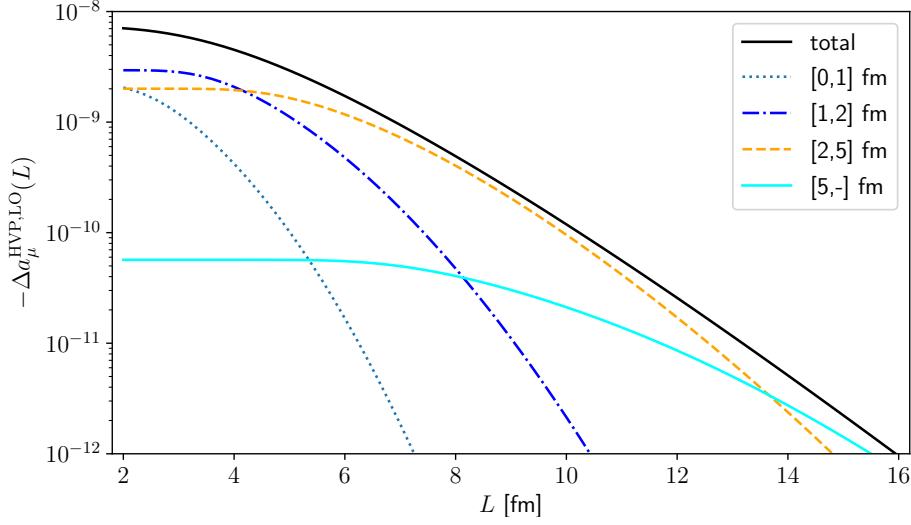


**Figure 3.**  $|\Delta a_\mu^{\text{HVP,LO}}(L)| = -\Delta a_\mu^{\text{HVP,LO}}(L)$  constructed from non-interacting pion correlator (3.9). The total (black curve) is divided into different Euclidean time contributions: [0,1] fm (dotted), [1,2] fm (dot-dashed), [2,5] fm (dashed) and [5,∞] fm (cyan). Pion mass  $m_\pi$  is set to 140 MeV.

$\tau \gtrsim L/4$ , the exponential suppression becomes weaker than  $\exp(-m_\pi L)$  due to a factor of  $L/4\tau$ , while for  $\tau \lesssim L/4$  the suppression is stronger. Thus, the effect on  $a_\mu^{\text{HVP,LO}}$  depends on which region of  $\tau$  one probes by the window quantity, for instance.

When  $\zeta$  is not so small, say  $\zeta > 0.05$ , the elliptic theta function is well approximated by  $\vartheta_3(0, \zeta) \sim \sqrt{\pi/(-\ln \zeta)}$  [28]. It means that the square brackets in (3.9) contains a term  $(4\pi\tau/m_\pi)^{3/2}(1/L)^3$  for relatively small volumes  $m_\pi L^2/4\tau \lesssim 3$ . It is remarkable that a power-law dependence shows up in the large-volume scaling:  $\sim 1/L^3$  for a fixed  $\tau$  or  $1/L^{3/2}$  for  $\tau \sim L$ .

Overall, the Euclidean correlator  $\Delta G(\tau, L)$  has a complex dependence on the volume and on the time separation. The scaling of  $a_\mu^{\text{HVP,LO}}$  could, therefore, be complicated as it is given by an weighted integral of  $G(\tau, L)$  over  $\tau$ . Namely, it may behave as power-law at relatively small  $L$ , say  $m_\pi L \sim 6$ , turn to exponential for larger  $L$ , and then decrease even faster for asymptotically large  $L$ . The explicit calculation is shown in the following.

### 3.2 Contribution $a_\mu^{\text{HVP,LO}}$

Let us define the finite-volume correction for  $a_\mu^{\text{HVP,LO}}$  as

$$\Delta a_\mu^{\text{HVP,LO}}(L) \equiv a_\mu^{\text{HVP,LO}}(L) - a_\mu^{\text{HVP,LO}}(\infty), \quad (3.10)$$

where  $a_\mu^{\text{HVP,LO}}(L)$  is obtained from the finite-volume Euclidean correlator  $G(\tau, L)$  using (2.5).

Figure 3 shows  $-\Delta a_\mu^{\text{HVP,LO}}(L)$  constructed from the non-interacting two-pion correlator (3.9), which is obtained under the assumption  $m_\pi\tau \gg 1$ . Since this condition is not always satisfied in the integral (2.5), we also show a decomposition of the integral

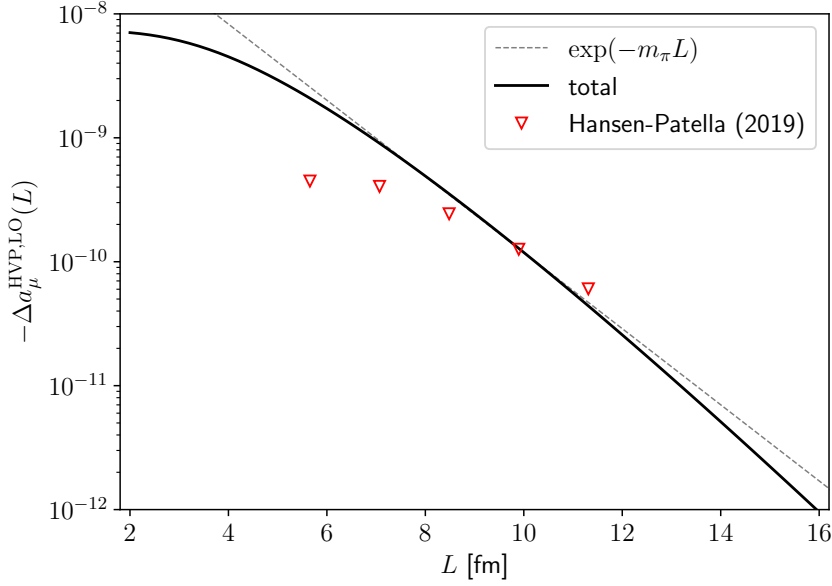


**Figure 4.**  $-\Delta a_\mu^{\text{HVP,LO}}(L)$  constructed from non-interacting pion correlator (3.9). An estimate by Hansen and Petella [7] (with an input  $F_\pi(s) = 1$ ) is shown by down-triangles. Also plotted is a line to show the slope of  $\exp(-m_\pi L)$  (dashed line).

into different regions of  $\tau$ . The different lines in Figure 3 represent contributions from a given Euclidean time range:  $[0,1]$  fm (dotted),  $[1,2]$  fm (dot-dashed),  $[2,5]$  fm (dashed) and  $[5,\infty]$  fm (cyan). The condition  $m_\pi \tau \gg 1$  would be satisfied reasonably well for  $\tau \simeq 2$  fm or larger. The finite-volume effect is negative and we plot  $-\Delta a_\mu^{\text{HVP,LO}}(L)$ .

The most significant contribution comes from the Euclidean time range  $[1,2]$  fm or  $[2,5]$  fm depending on the volume size  $L$ . Namely, the range  $[1,2]$  fm is dominant for  $L \lesssim 4$  fm, while the other range  $[2,5]$  fm becomes far more important beyond  $L \sim 5$  fm. Note that  $a_\mu^{\text{HVP,LO}}$  itself is dominated by the time interval  $\sim 1/m_\mu$ , which is typically around 1–2 fm.

One also finds that  $-\Delta a_\mu^{\text{HVP,LO}}(L)$  decreases faster than exponential for large  $L$ . The curve for each time range shows a curvature, most prominently for the smallest time range,  $[0,1]$  fm, but for others too. This is understood from the asymptotic form of (3.9), *i.e.*  $\exp(-m_\pi L^2/4\tau)$  with  $\tau$  in the limited range. Since the integral (2.5) is dominated by the time range around  $1/m_\mu$ , one might think that the finite-volume effect scales as  $\exp(-m_\pi m_\mu L^2/4)$  for asymptotically large  $L$ , but the explicit calculation shows a more complicated convolution of different time separations as demonstrated in the plot.

For smaller  $L$  region, on the other hand, the decrease of  $|\Delta a_\mu^{\text{HVP,LO}}(L)|$  towards larger volumes is much flatter, suggesting non-exponential or power-like behavior. It is again consistent with the expectation from the functional form of the correlator as discussed above.

In Figure 4 the total  $-\Delta a_\mu^{\text{HVP,LO}}(L)$  is compared with the previous result by Hansen

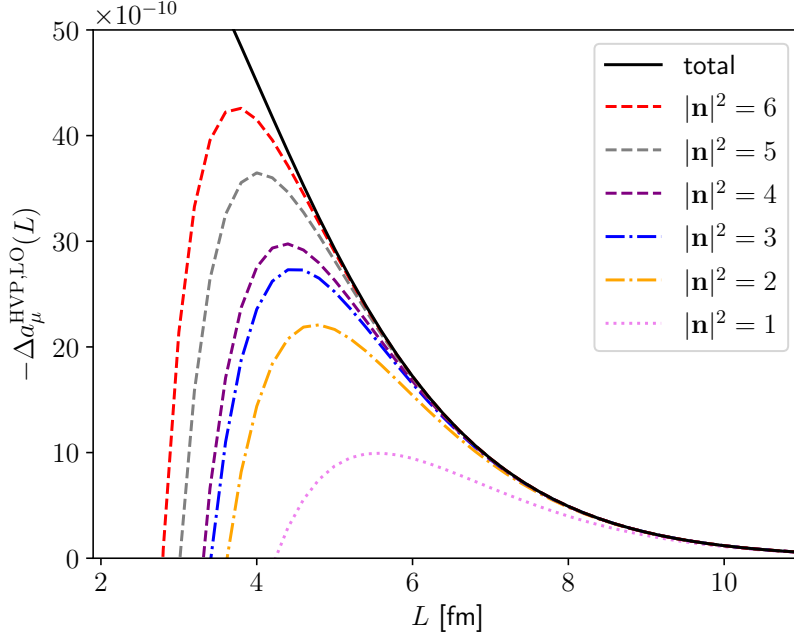


**Figure 5.**  $-\Delta a_\mu^{\text{HVP,LO}}(L)$  constructed from non-interacting pion correlator (3.9). The contributions of wrap-around effects are added only up to a certain value of  $|\mathbf{n}|^2$ .

and Petella [7] (with  $F_\pi(s) = 1$ ). Our estimate is close to Hansen-Patella for  $L \simeq 8$ –10 fm, but decreases more rapidly for large  $L$  and increases more significantly toward smaller volumes. Also shown in Figure 4 is a line showing the slope of  $\exp(-m_\pi L)$  as suggested in [7]. The magnitude of this exponential line is tuned such that it runs through the point near  $L = 10$  fm. The estimate based on non-interacting pions shows a significantly different dependence on  $L$  from the simple exponential suggested in previous studies.

In chiral perturbation theory, the finite-volume effect is often estimated with a truncated sum over the integers  $\mathbf{n}$  in (3.3) that represent how many times pions wrap around the volume in each direction. For each  $|\mathbf{n}|$ , the  $L$ -dependence is given by  $e^{-m_\pi |\mathbf{n}| L} / \sqrt{m_\pi |\mathbf{n}| L}$  [3, 5], and the total is obtained by a sum over  $|\mathbf{n}|$  taking into account a multiplicity for each  $|\mathbf{n}|$ . Figure 5 demonstrates the effect of the truncation. We again use the approximation  $m_\pi \tau \gg 1$ , and the two-point function is given by (3.9). It turns out that the truncation at  $|\mathbf{n}| = 1$  leads to a significant underestimate even at  $L \sim 6$  fm or 8 fm. The higher-order effects are also numerically important, although not very visible in this logarithmic plot. This plot is obtained with the approximation  $m_\pi \tau \gg 1$ , but similar results would be expected for the full estimate.

The same quantity  $-\Delta a_\mu^{\text{HVP,LO}}(L)$ , without the truncation in  $|\mathbf{n}|$ , is plotted as a function of  $1/(m_\pi L)^2$  in Figure 6. Near the infinite volume limit, the finite-volume correction vanishes exponentially or even faster as described above, while it increases significantly for finite volumes from  $1/(m_\pi L)^2 \sim 0.03$ , which corresponds to  $m_\pi L \simeq 6$ . It looks as if the increase is linear in  $1/(m_\pi L)^2$ , but the actual functional form would be complex, *i.e.* a

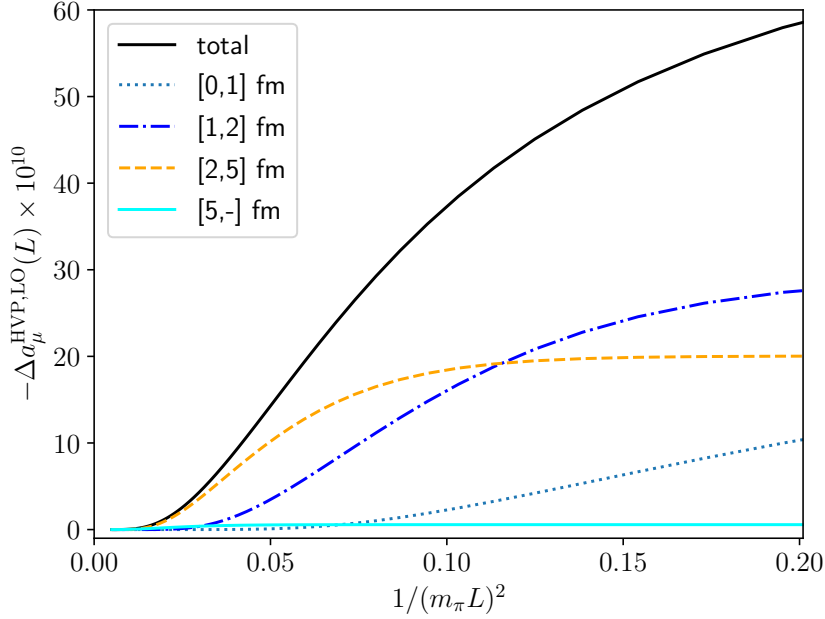


**Figure 6.**  $-\Delta a_\mu^{\text{HVP,LO}}(L)$  constructed from non-interacting pion correlator (3.9) as a function of  $1/(m_\pi L)^2$ . Different lines are represented as in Figure 3.

mixture of different powers  $L^\alpha$  as discussed in the previous subsection.

The overall size, of the order of  $20 \times 10^{-10}$  at the nominal volume size  $m_\pi L \simeq 4$ , or  $1/(m_\pi L)^2 \simeq 0.06$ , is very significant compared to the target precision of about a few times  $10^{-10}$ .

## 4 Two-pion contribution in the interacting case

In this section, we extend the estimate of the finite-volume effects to the case of interacting pions. Instead of performing lattice QCD simulations, which is computationally expensive, we use the phenomenologically known  $\pi\pi$  phase shift  $\delta_1^1(\mathbf{k})$  and time-like pion form factor  $F_\pi(s)$  to construct the Euclidean correlator. In doing so, we neglect the inelastic effects due to four-pion states and higher, since their contribution to  $a_\mu^{\text{HVP,LO}}$  is sub-leading (10% or less compared to the  $\pi\pi$  contribution) and so is the finite-volume effect. The Euclidean correlator (2.8) on a finite volume is constructed from the energy spectrum  $E_{\pi\pi,n}$  and the matrix element  $\langle 0 | j_z^{\text{em}} | \pi\pi, n \rangle_V$ . They are obtained by applying Lüscher's condition for finite-volume states.

### 4.1 Finite-volume energy spectrum

Two-pion spectrum on a finite volume satisfies Lüscher's condition [9]:

$$\delta(k) + \phi\left(\frac{kL}{2\pi}\right) = n\pi, \quad (4.1)$$

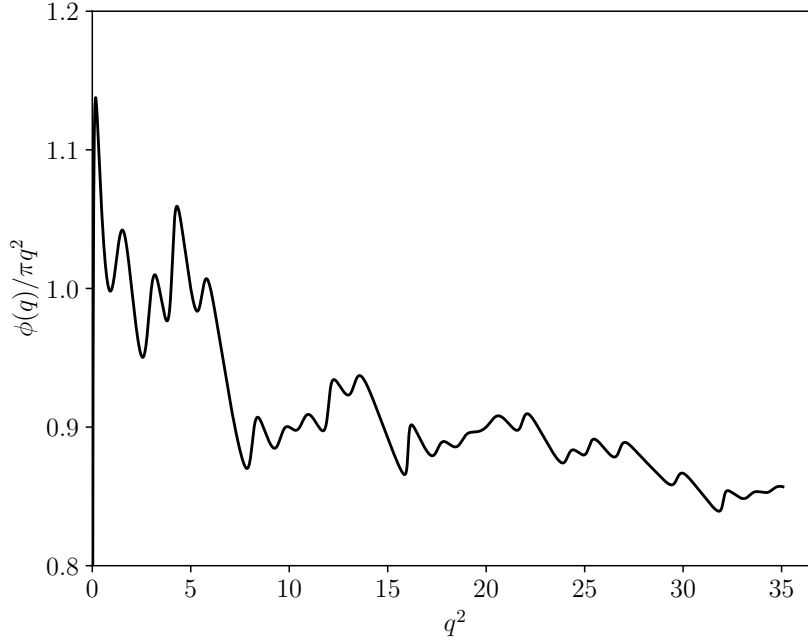


**Figure 7.**  $\phi(q)/\pi q^2$  computed for  $q^2$  up to 35.0.

where  $k \equiv |\mathbf{k}|$  and  $\delta(k)$  is a short-hand notation of  $\delta_1^1(\mathbf{k})$  for the present case of  $I = J = 1$ . The two-pion state energy to satisfy (4.1) is obtained as  $E_{\pi\pi,n} = 2\sqrt{m_\pi^2 + k^2}$  from  $k$  for each  $n$ . The function  $\phi(q)$  is defined by  $\tan \phi(q) = -\pi^{3/2}q/\mathcal{Z}_{00}(1;q)$  with Lüscher's generalized zeta function  $\mathcal{Z}_{00}(s;q) = (1/\sqrt{4\pi}) \sum_{\mathbf{l}} (\mathbf{l}^2 - q^2)^{-s}$ . On the right-hand side of (4.1),  $n$  is a non-negative integer.

We compute  $\phi(q)$  numerically up to  $q = \sqrt{35.0} \approx 5.9$ , beyond which we face a numerical instability. We follow the prescription given in the Appendix C of [9], and the results are confirmed with the numerical table in [29] for  $q^2 = 0.1$ –9.0. Near  $q^2 = 0$ , especially below 0.1, our calculation of  $\phi(q)$  agrees with (A.4) and (A.5) of [29]. The results for  $\phi(q)/\pi q^2$  are shown in Figure 7. It is close to 1 at the first approximation, but a complicated structure is visible. In the following analysis,  $n$  is limited to  $n \leq 26$ , which means that the highest energy  $\pi\pi$  state for a given volume is limited. We also assume that the contribution of higher partial waves of  $l \geq 3$  can be ignored.

Figure 8 shows the energy spectrum of the  $\pi\pi$  states on finite volumes. The  $\pi\pi$  phase shift  $\delta(k)$  for those of interacting spectrum (blue lines) is taken from Gounaris-Sakurai model (see below). Non-interacting  $\pi\pi$  spectrum is also shown (orange dotted lines), which is obtained by setting  $\delta(k) = 0$ . The highest energy state possible with  $n \leq 26$  is slightly below 1,200 MeV at  $L = 12$  fm, while the covered energy range extends much higher for smaller volumes.

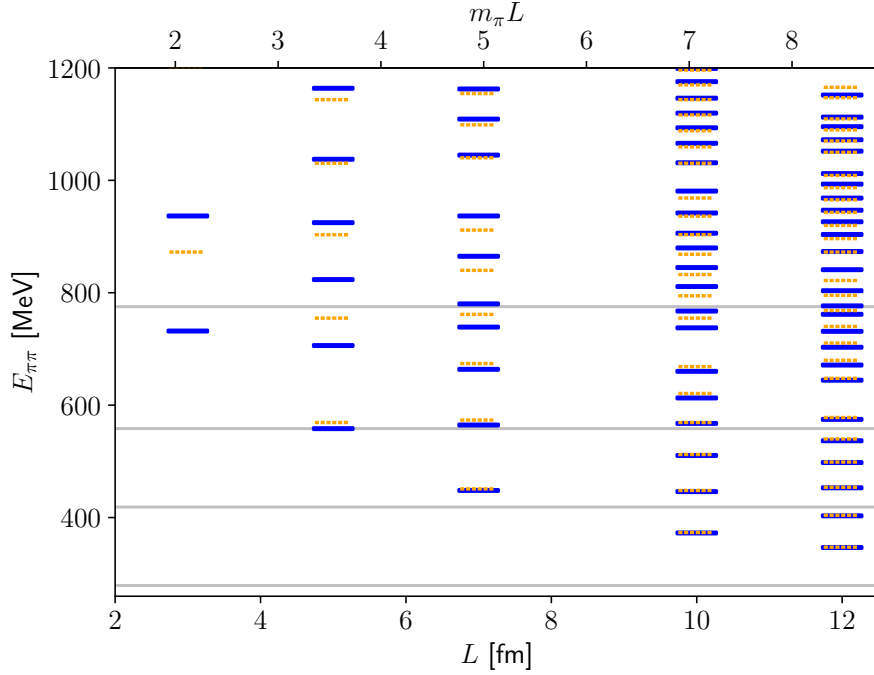


**Figure 8.** Energy spectrum of the  $\pi\pi$  states on finite volumes of size  $L = 3, 5, 7, 10$  and  $12$  fm. The spectrum with (blue lines) and without (orange dotted)  $\pi\pi$  interaction is shown for each volume. Gray lines correspond to  $2m_\pi$ ,  $3m_\pi$ ,  $4m_\pi$ , and  $m_\rho$ , from the bottom to top. The pion and rho meson masses are set to their physical values:  $m_\pi = 139.6$  MeV,  $m_\rho = 775$  MeV.

#### 4.2 Matrix element from Gounaris-Sakurai model

The matrix element  $\langle 0 | j_z^{\text{em}} | \pi\pi, n \rangle_V$  is reconstructed from the electromagnetic pion form factor  $|F_\pi(s)|$  with Lellouch-Lüscher formula [10, 11] as described in [12]:

$$|F_\pi(E_{\pi\pi,n}^2)|^2 = \left( q\phi'(q) + k \frac{\partial \delta(k)}{\partial k} \right) \frac{3\pi E_{\pi\pi,n}^2}{2k^5} |\langle 0 | j_z^{\text{em}} | \pi\pi, n \rangle_V|^2. \quad (4.2)$$

We assume the Gounaris-Sakurai (GS) model [14] for the pion form factor. It is written as

$$F_\pi^{\text{GS}}(s) = \frac{-m_\rho^2 - \Pi_\rho(0)}{s - m_\rho^2 - \Pi_\rho(s)}, \quad (4.3)$$

where  $\Pi_\rho(s)$  represents the  $\rho$  meson self-energy as defined in the model. In the GS model,  $\Pi_\rho(s)$  is obtained using the (twice-subtracted) dispersion relation with an input

$$\text{Im}\Pi_\rho(s) = -\frac{g_{\rho\pi\pi}^2}{6\pi} \frac{k^3}{\sqrt{s}}, \quad (4.4)$$

where  $k = \sqrt{s/4 - m_\pi^2}$ . The  $\rho\pi\pi$  coupling  $g_{\rho\pi\pi}$  is set using the experimentally available  $\rho \rightarrow \pi\pi$  decay width as  $\Gamma_{\rho\pi\pi} = (g_{\rho\pi\pi}^2/6\pi)(k_\rho^3/m_\rho^2)$ . In this analysis, we took  $\Gamma_{\rho\pi\pi} = 149$  MeV, which corresponds to  $g_{\rho\pi\pi} = 5.976$ .

The pion form factor (4.2) has a peak at the physical  $\rho$ -meson mass as shown in Figure 9. The sudden drop near the peak due the  $\rho$ - $\omega$  mixing is not captured by the GS

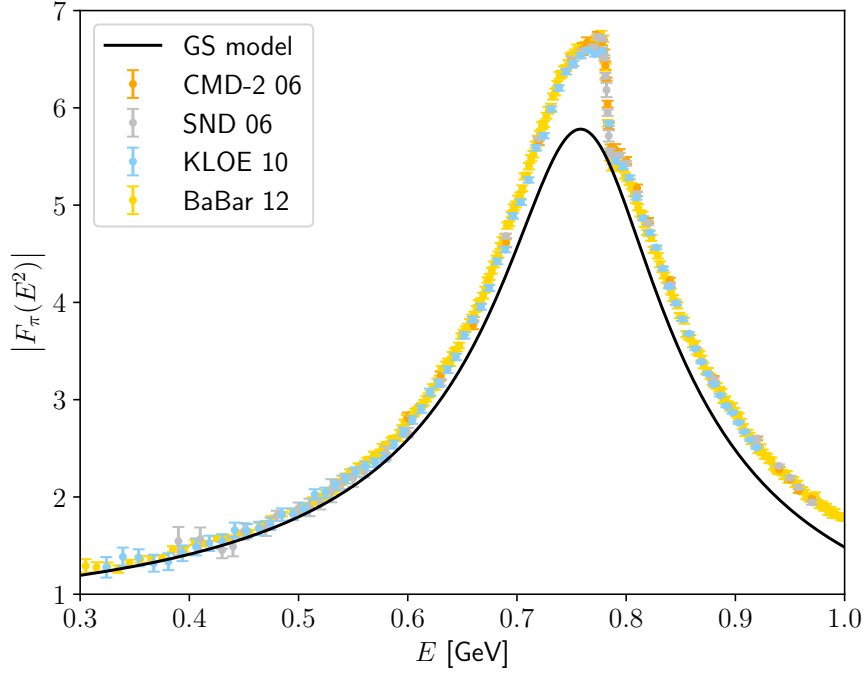


**Figure 9.** Time-like pion form factor from the experimental data of  $e^+e^- \rightarrow \pi^+\pi^-$  (CMD-2 06 [30, 31], SND 06 [32], KLOE [33], BaBar [34]) and from Gounaris-Sakurai (GS) model (solid line).

model (black curve), which contains the  $I = 1$  states only, but the overall shape of the experimental data is well reproduced. The deficit of the GS model (black curve) compared to the experimental data is mainly attributed to the inelastic states [35, 36]. Since  $|F_\pi(s)|$  is greatly enhanced due to the  $\rho$  resonance, the contribution to  $a_\mu^{\text{HVP,LO}}$  is also expected to be much larger compared to the non-interacting case  $|F_\pi(s)| = 1$ .

The phase shift  $\delta(k)$  in the GS model is written as

$$\frac{k^3}{\sqrt{s}} \cot \delta(k) = k^2 h(\sqrt{s}) - k_\rho^2 h(m_\rho) + b(k^2 - k_\rho^2), \quad (4.5)$$

where  $k_\rho = \sqrt{m_\rho^2/4 - m_\pi^2}$ . The function  $h(\sqrt{s})$  and a constant  $b$  are written as

$$h(\sqrt{s}) = \frac{2}{\pi} \frac{k}{\sqrt{s}} \ln \left( \frac{\sqrt{s} + 2k}{2m_\pi} \right), \quad (4.6)$$

$$b = -h(m_\rho) - \frac{24\pi}{g_{\rho\pi\pi}^2} - \frac{2k_\rho^2}{m_\rho} \frac{dh}{d\sqrt{s}} \Big|_{\sqrt{s}=m_\rho}, \quad (4.7)$$

and the  $\rho$  meson mass is set with the condition

$$\text{Re}\Pi_\rho(s)|_{s=m_\rho^2} = 0, \quad \frac{d}{ds}\text{Re}\Pi_\rho(s) \Big|_{s=m_\rho^2} = 0. \quad (4.8)$$

Some details of the Gounaris-Sakurai model are found in the Appendix A of [16].

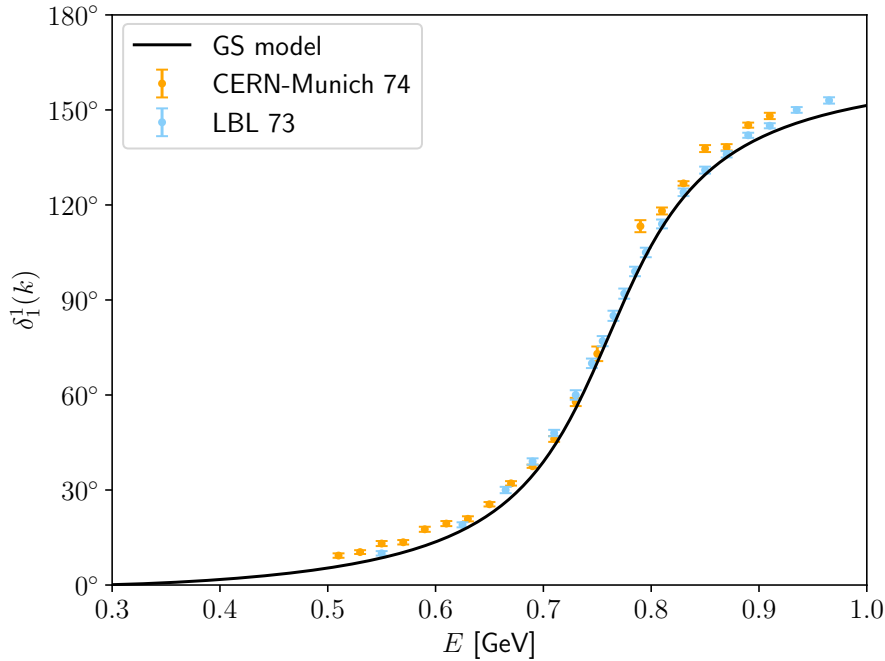


**Figure 10.** Phase shift from the experimental data (CERN-Munich 74 [37] and LBL 73 [38]), compared with Gounaris-Sakurai (GS) model (solid line).

Figure 10 shows the experimental data for  $\delta(k) = \delta_1^1(k)$  and the corresponding GS model. The phase shift passes through  $90^\circ$  around the mass of the  $\rho$  meson. The GS model describes the experimental data quite closely.

### 4.3 Sum over the low-lying $\pi\pi$ states

We reconstruct the finite-volume Euclidean correlator  $G(\tau, L)$  using (2.8) with finite-volume energy  $E_{\pi\pi, n}$  and matrix element  $\langle 0 | j_z^{\text{em}} | \pi\pi, n \rangle_V$  as described above. Since the major contribution to  $a_\mu^{\text{HVP, LO}}(L)$  arises from energy levels that are not too high compared to  $m_\mu$  due to the suppression of the kernel function  $K_E(Q^2)$  in large  $Q^2$ , we expect that the sum over  $n$  saturates rapidly beyond  $E_{\pi\pi} \sim 1$  GeV. The finite-volume effect  $\Delta a_\mu^{\text{HVP, LO}}(L)$  should be even more dominated by low-energy states.

In Figure 11 we plot  $a_\mu^{\text{HVP, LO}}(L)$  constructed from a finite number of low-lying  $\pi\pi$  states. That is, the sum (2.8) is truncated at an upper limit  $n = 3, 5, 10, 20$  and  $26$  when constructing the finite-volume correlator  $G(\tau, L)$ . The  $\tau$  integral is divided into  $[0, 1]$  fm (top panel),  $[1, 2]$  fm (middle) and  $[2, 10]$  fm (bottom) as in the analysis of the non-interacting case. The estimate of  $a_\mu^{\text{HVP, LO}}(L)$  is well saturated by a smaller number of states, even 3 or 5, for smaller volumes,  $L \sim 3\text{--}4$  fm, as expected from the corresponding energy spectrum (Figure 8), *i.e.* the energy of the fifth lowest state is already above 1 GeV for  $L = 3$  fm and 5 fm. Going to larger volumes, the saturation becomes slower, but we find that the differences between  $n = 20$  and  $26$  are very small: symbols (open and filled circles) are nearly overlapping in the plot. Numerically, the difference between  $n = 20$  and  $26$  is as



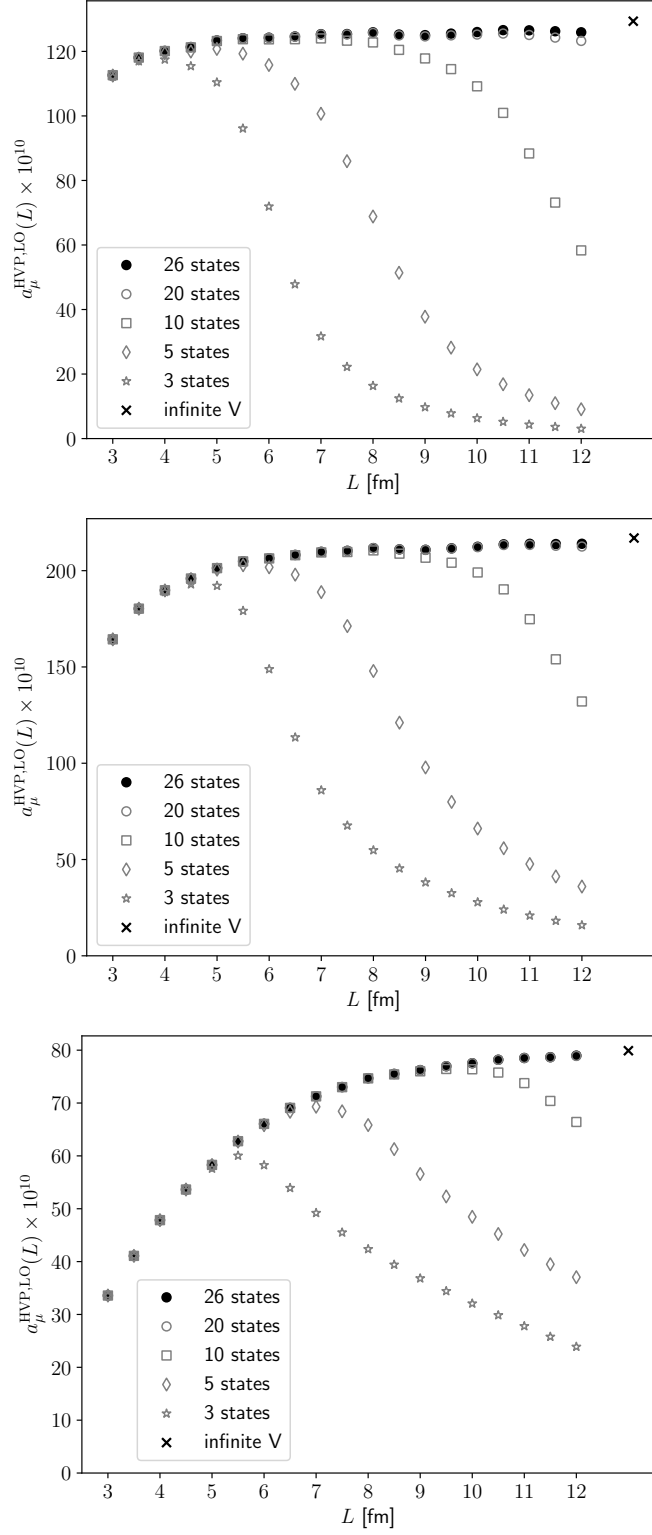


**Figure 11.** Saturation of the sum over  $\pi\pi$  states for  $a_\mu^{\text{HVP,LO}}(L)$ . Lowest  $n$  states are summed to construct the correlator  $G(\tau, L)$ :  $n = 3, 5, 10, 20$  and  $26$ . Results for partial time integrals in the range  $[0,1]$  fm (top panel),  $[1,2]$  fm (middle),  $[2,10]$  fm (bottom) are shown as a function of  $L$ . Crosses represents the infinite volume limit including all possible states.

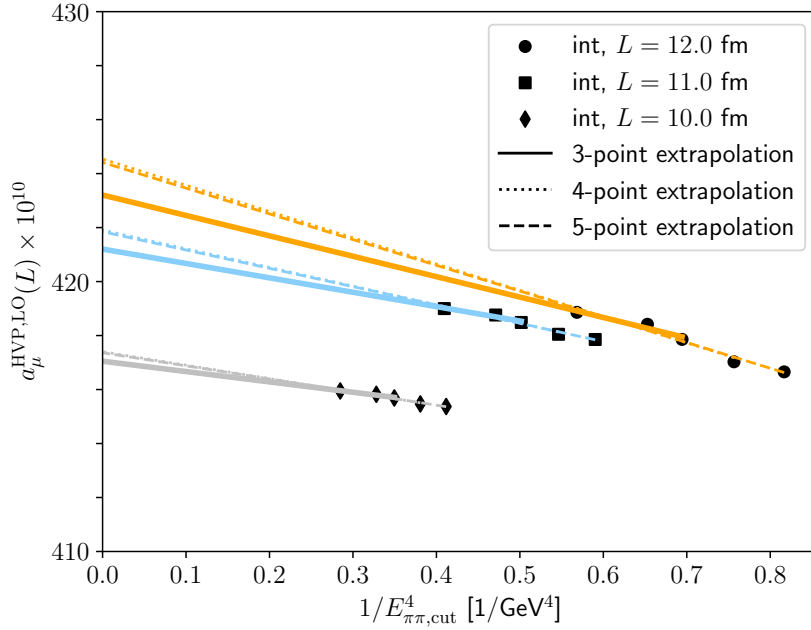


**Figure 12.**  $a_\mu^{\text{HVP,LO}}(L)$  reconstructed with a truncated sum over states in (2.8). Results for  $L = 12$  fm (circles), 11 fm (squares) and 10 fm (diamonds) with  $\tau_c = 10$  fm are plotted as a function of  $1/E_{\pi\pi,\text{cut}}^4$ , where  $E_{\pi\pi,\text{cut}}$  is the highest energy  $E_{\pi\pi,n}$  included. Data points correspond to  $n = 22$ –26 (from right to left). A  $\chi^2$ -fit as a linear function of  $1/E_{\pi\pi,\text{cut}}^4$  yields the lines. Solid, dotted and dashed lines represent the results with the highest 3, 4, and 5  $E_{\pi\pi,\text{cut}}$  points, respectively.

small as  $3 \times 10^{-10}$ ,  $4 \times 10^{-10}$ ,  $4 \times 10^{-10}$  for the time ranges  $[0,1]$  fm,  $[1,2]$  fm and  $[2,10]$  fm, respectively, even at the worst case of  $L = 12$  fm. For smaller volumes, the difference is even smaller.

The dependence on the upper limit of the energy sum,  $E_{\pi\pi,\text{cut}}$ , is expected to be  $1/E_{\pi\pi,\text{cut}}^4$ , since the kernel function  $K_E(Q^2)$  in (2.1) scales as  $1/(Q^2)^3$  for large  $Q^2$ . We therefore extrapolate the results for  $a_\mu^{\text{HVP,LO}}(L)$  towards  $n \rightarrow \infty$  assuming the scaling  $C_0 - C_1/E_{\pi\pi,\text{cut}}^4$ . In practice, we fit 3–5 data points of the highest  $E_{\pi\pi,\text{cut}}$  with this scaling form (taking  $E_{\pi\pi,\text{cut}} = E_{\pi\pi,n}$ ) and obtain the estimate of  $a_\mu^{\text{HVP,LO}}(L)$  from  $C_0$ . This extrapolation is shown in Figure 12. The fit results of 3–5 points slightly deviate, but their size is only about  $1 \times 10^{-10}$  for the worst case of  $L = 12$  fm and much smaller for smaller volumes, 11 fm and 10 fm. In the following, we take the extrapolated values for  $a_\mu^{\text{HVP,LO}}(L)$  with three highest data points as our central values, as the energy scaling is obtained for asymptotically large energies. The lowest energy involved in the extrapolation is about 1.1 GeV for  $L = 12$  fm. We treat the deviation of 4- or 5-point fit as an estimate of systematic error. This estimate of error is added for both directions, positive and negative, to be conservative.

The infinite volume limit to compare (crosses in Figure 11) is obtained using the Euclidean correlator directly reconstructed from the pion form factor :

$$G(\tau) = \int_0^\infty dE E^2 \rho(E^2) e^{-E\tau}, \quad (4.9)$$

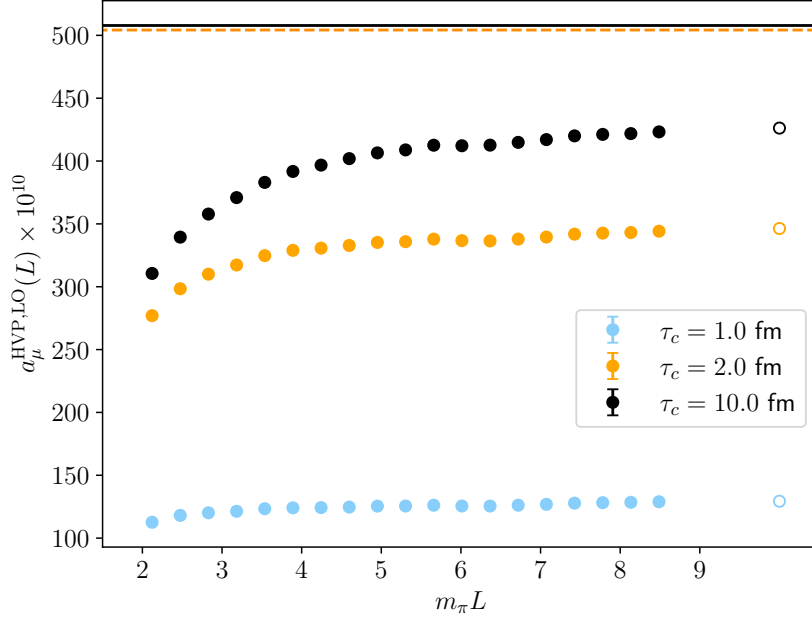


**Figure 13.**  $\pi\pi$  contribution to  $a_\mu^{\text{HVP,LO}}$  for different volumes. The results for three different time integral upper limit are shown, *i.e.*  $\tau_c = 1$  fm, 2 fm and 10 fm. The infinite volume results are shown on the right by open symbols for each  $\tau_c$ . Two horizontal lines represent the estimates from dispersion analysis (solid line: DHMZ 19 [39], dashed line: KNT 19 [40]).

where

$$\rho(E^2) = \frac{1}{48\pi^2} \left(1 - \frac{4m_\pi^2}{E^2}\right)^{3/2} |F_\pi^{\text{GS}}(E)|^2 \quad (4.10)$$

is the spectral function representing the  $\pi\pi$  states.

#### 4.4 Results for $a_\mu^{\text{HVP,LO}}$

Results from the decomposition (2.8) for  $a_\mu^{\text{HVP,LO}}$  are shown in Figure 13. The results are shown for different values of the upper limit  $\tau_c$  in the time-momentum integral (2.5):  $\tau_c = 1$  fm, 2 fm and 10 fm. For the largest volumes, beyond  $m_\pi L \gtrsim 6$ , we find that the finite-volume estimate is already close (within roughly  $15 \times 10^{-10}$ ) to the infinite volume limit (open circles).

In the same plot, the estimates from the dispersion relation using the experimental data of  $e^+e^- \rightarrow \pi^+\pi^-$  are shown by horizontal lines; two groups, DHMZ 19 [39] and KNT 19 [40], are consistent with each other. The results of our analysis are significantly lower even with the largest  $\tau_c = 10$  fm, for which the integral has almost reached the value of  $\tau_c \rightarrow \infty$ . In fact, the difference between  $\tau_c = 5$  fm and 10 fm is invisible at the scale of this plot. The deficit compared to the dispersion method is attributed to the GS model for the pion form factor. As shown in Figure 9, the GS model significantly underestimates the experimental data near the  $\rho$  resonance as it ignores  $\rho$ - $\omega$  mixing coming from isospin breaking. This inconsistency, however, would not largely affect our analysis of finite-volume effects since

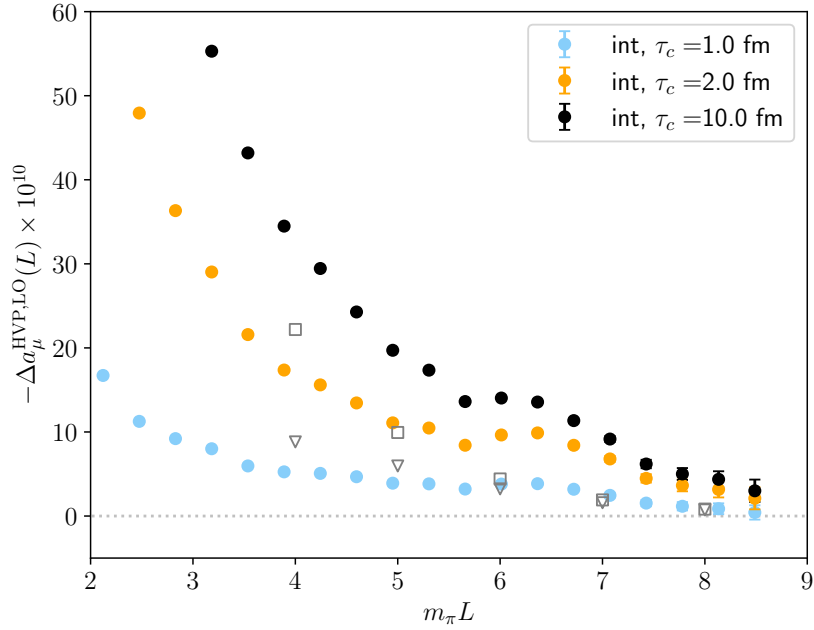


**Figure 14.** Finite volume effect for the muon anomalous magnetic moment  $-\Delta a_\mu^{\text{HVP,LO}}(L)$ . Estimate obtained with phenomenological  $\pi\pi$  phase shift and time-like pion form factor described by the Gounaris-Sakurai model. Results are plotted for three values of upper limit  $\tau_c$  in the Euclidean time integral (2.5):  $\tau_c = 1$  fm, 2 fm and 10 fm. The time integral is nearly saturated for  $\tau_c = 10$  fm. Estimates by Hansen and Patella [7, 8] are also plotted (triangles: leading order,  $e^{-m_\pi L}$  [7], squares: including up to  $e^{-3m_\pi L}$  [8]).

the agreement of the pion form factor is better in the lower-energy region, which is most responsible for finite-volume effects.

Figure 13 clearly shows that the finite volume effect is significant for  $m_\pi L \lesssim 6$ , which corresponds to  $L \lesssim 8$  fm, especially when the large time separation,  $\gtrsim 1$  fm, is included in the integral (2.5). In the following section, we analyse the finite-volume effect  $\Delta a_\mu^{\text{HVP,LO}}$  in more details.

## 5 Finite volume effects for $a_\mu^{\text{HVP,LO}}$

In this section, we present our estimate of finite-volume effects for  $a_\mu^{\text{HVP,LO}}$ . The results for the total and sharply cut time windows are shown first, and those for the smeared windows follow.

### 5.1 Total, and sharply cut time windows

Figure 14 shows the finite-volume effect  $-\Delta a_\mu^{\text{HVP,LO}}(L)$  as a function of  $m_\pi L$ . The infinite-volume limit constructed with (4.9) is subtracted from the finite-volume results shown in Figure 13.

The finite-volume effect  $-\Delta a_\mu^{\text{HVP,LO}}(L)$  increases rapidly for  $m_\pi L \simeq 6$  or smaller, especially when a region of large Euclidean time separation is included ( $\tau_c = 2$  fm and

10 fm). The size of  $-\Delta a_\mu^{\text{HVP,LO}}(L)$  is as large as  $35 \times 10^{-10}$  for  $m_\pi L = 4$ , which is often considered a safe choice to suppress the systematic error due to the finite volume size. The target precision for  $a_\mu^{\text{HVP,LO}}$  is, however, very high, *i.e.* at the level of  $5 \times 10^{-10}$  or better, so that the size of the systematic effect as we find here has to be carefully estimated and subtracted.

The integral in the time-momentum representation (2.5) is saturated to an excellent precision at  $\tau_c = 10$  fm (black points in Figure 14), and these data points can be considered an estimate of the total  $-\Delta a_\mu^{\text{HVP,LO}}(L)$ .

One may wonder why  $-\Delta a_\mu^{\text{HVP,LO}}(L)$  develops a bump between  $m_\pi L = 6$  and 7 especially for  $\tau_c = 2$  fm and 10 fm. In this region, the estimate is dominated by the lowest 10  $\pi\pi$ -energy states, as can be seen in Figure 11 where the saturation of  $a_\mu^{\text{HVP,LO}}(L)$  is plotted. (The corresponding range of  $L$  is about 9–10 fm.) These lowest 10 modes cover the range of the  $\rho$  meson resonance (see Figure 8), where the time-like pion form factor  $F_\pi(s)$  sharply peaks. It enters the formula as  $|F_\pi(s)|^2$ , and its maximum value is about 35, a very significant enhancement compared to  $|F_\pi(0)|^2 = 1$ . The bump as seen in Figure 14 can be generated depending on whether one of the discrete energy modes lies on top of the resonance or on its shoulders. It suggests the importance to include the non-perturbative resonance effects in the estimate of the finite-volume effect.

The estimates of Hansen and Patella using effective field theory [7, 8] are also plotted in Figure 14. They involve a wrap-around effect of the pion in one direction giving  $e^{-m_\pi L}$  [7] (triangles), as well as those involving multiple wraps up to the term of  $e^{-3m_\pi L}$  [8] (squares). (Contributions of order  $e^{-\sqrt{2+\sqrt{3}}m_\pi L}$  are neglected, though. It is therefore effectively summed up to  $e^{-\sqrt{3}m_\pi L}$ .) These points can be compared with the full  $-\Delta a_\mu^{\text{HVP,LO}}(L)$ , *i.e.* our estimate at  $\tau_c = 10$  fm. Our estimate turns out to be significantly larger and slower to converge to zero for large volumes. This is likely due to the  $\rho$ -meson resonance enhancement present in our analysis, as discussed above. The most pronounced difference is seen in the region of  $m_\pi L = 6$ –7 and around it, which is exactly the point where the above-mentioned effect of the resonance enhancement becomes significant. The ChPT, or the calculation based on the space-like momentum region in general, cannot precisely capture the resonance structure.

In the BMW calculation [1], the finite-volume effect is estimated in two steps. Their reference lattice has a size  $L_{\text{ref}} \simeq 6.3$  fm, which corresponds to  $m_\pi L_{\text{ref}} \simeq 4.4$ . From there, they estimate the difference from a bigger volume of  $L_{\text{big}} \simeq 10.8$  fm ( $m_\pi L_{\text{big}} \simeq 7.6$ ), and then use chiral effective theory [8] to estimate the difference from the infinite volume. The first step,  $L_{\text{ref}}$  to  $L_{\text{big}}$ , is estimated as  $18(2) \times 10^{-10}$  mainly using actual simulation data on a coarse lattice, while the second is smaller than  $1 \times 10^{-10}$ . Our corresponding estimates are  $21.5 \times 10^{-10}$  and  $5.5 \times 10^{-10}$ , respectively. We find a reasonable agreement for the former,  $L_{\text{ref}} \rightarrow L_{\text{big}}$ , while the estimate for  $L_{\text{big}}$  is much larger in our analysis. This probably originates from the underestimate with the chiral effective theory, as mentioned above.

In the more recent publication [22], the estimate for  $L_{\text{ref}} \rightarrow L_{\text{big}}$  from actual simulations is updated to  $9.3(8) \times 10^{-10}$ . Their own estimate for  $L_{\text{ref}} \rightarrow \infty$  is also updated using a method similar to our work but with the pion form factor driven from Omnes formula as

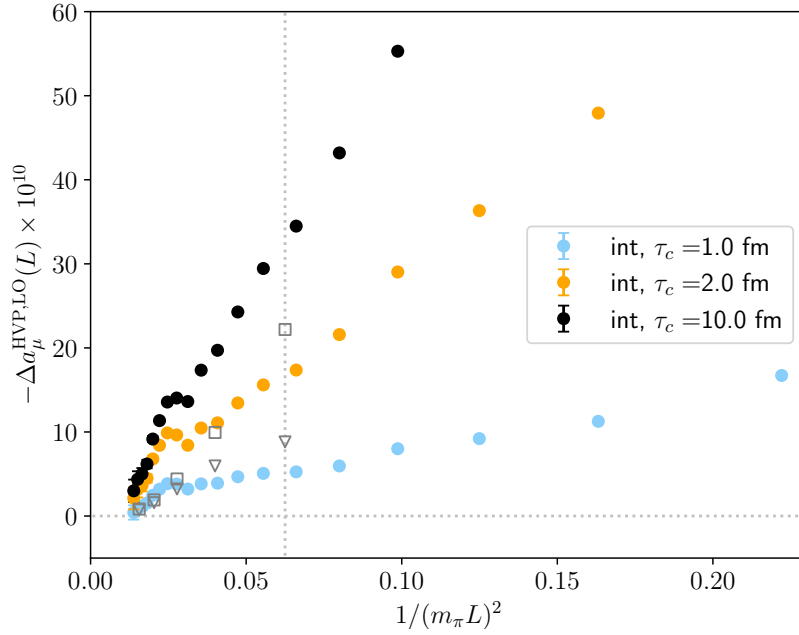


**Figure 15.** Finite volume effect for the muon anomalous magnetic moment  $-\Delta a_\mu^{\text{HVP,LO}}(L)$  plotted as a function of  $1/(m_\pi L)^2$ . The vertical dotted line shows  $m_\pi L = 4$ . Other details are the same as in Figure 14.

$9.1(2) \times 10^{-10}$ , which is much smaller than our analysis  $22.5 \times 10^{-10}$ . The differences are to be understood in detail.

In the recent calculation by the RBC/UKQCD collaboration [26] the largest volume lattice at the physical point has  $m_\pi L = 5.2$ , for which we expect a correction of about  $18.1 \times 10^{-10}$ .

The same results for  $-\Delta a_\mu^{\text{HVP,LO}}(L)$  are plotted as a function of  $1/(m_\pi L)^2$  in Figure 15. Away from the large-volume regime,  $1/(m_\pi L)^2 \gtrsim 0.04$ , the finite-volume correction seems well described by a linear function of  $1/(m_\pi L)^2$ , independent of  $\tau_c$ . Closer to the infinite volume limit,  $1/(m_\pi L)^2 \sim 0.025$ , however, they clearly deviate from the linear dependence and approach zero very rapidly. This behavior resembles that of the non-interacting pion case (see Figure 6).

To see this explicitly, we show a comparison between the finite-volume effect with and without the  $\pi\pi$  interactions in Figure 16. The plots represent the contributions in the Euclidean time range  $[1,2]$  fm (top panel) and  $[2,10]$  fm (bottom panel). The non-interacting  $\pi\pi$  contribution (squares) is evaluated numerically with inputs  $\delta(k) = 0$  and  $F_\pi(s) = 1$  and no additional approximation such as  $m_\pi \tau \gg 1$  is involved. It can be compared with an evaluation with the approximate formula (3.9) for  $m_\pi \tau \gg 1$  (as shown in Figure 6). We find a reasonable agreement for their size and overall shape. Including  $\pi\pi$  interactions, the estimate for  $-\Delta a_\mu^{\text{HVP,LO}}(L)$  becomes significantly larger, due to the  $\rho$ -meson resonance enhancement of  $|F_\pi(s)|$ .

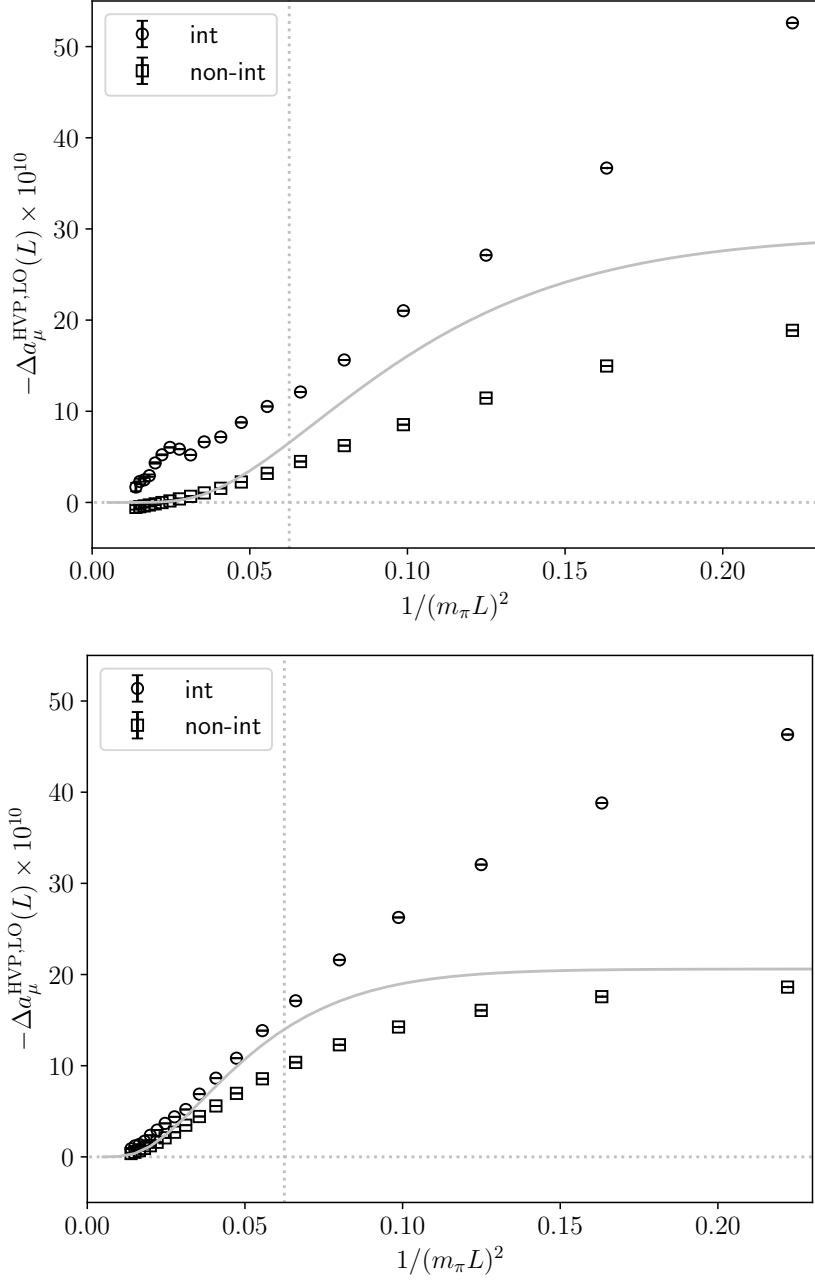


**Figure 16.** Finite volume effect for  $a_\mu^{\text{HVP, LO}}$  evaluated in the time range  $[1, 2]$  fm (top panel) and in  $[2, 10]$  fm (bottom panel). Estimates with and without  $\pi\pi$  interactions are shown (circles and squares, respectively). The error bar is from the extrapolation in the energy cutoff  $E_{\pi\pi, \text{cut}}$  (see Section 4.3). The gray curve is obtained with the approximate formula for non-interacting  $\Delta G(\tau, L)$ , Eq.(3.9), that is valid for  $m_\pi \tau \gg 1$ .

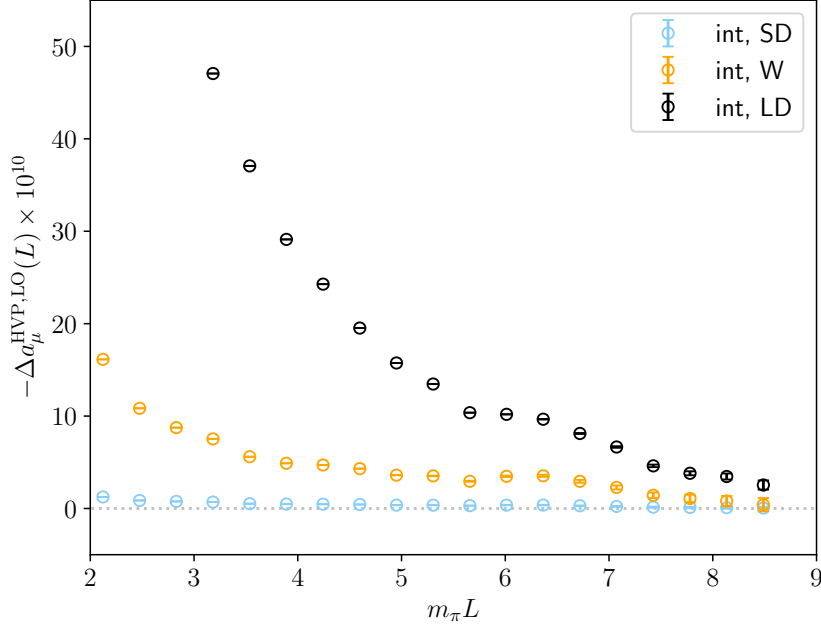


**Figure 17.** Finite-volume effect for  $a_\mu^{\text{HVP,LO}}$  evaluated for different Euclidean time windows, plotted as a function of  $m_\pi L$ . The error bar is from the extrapolation in the energy cutoff  $E_{\pi\pi,\text{cut}}$  (see Section 4.3).

## 5.2 Smeared time windows

For convenience, we also provide the results for the smeared time windows proposed by [20] and commonly adopted by many collaborations. Using the smeared Heaviside function

$$\Theta(\tau, \tau'; \Delta) \equiv \frac{1}{2} \left[ 1 + \tanh \frac{\tau - \tau'}{\Delta} \right], \quad (5.1)$$

the leading-order HVP contribution  $a_\mu^{\text{HVP,LO}}$  can be decomposed into short-distance (SD), window (W) and long-distance (LD) pieces as  $a_\mu^{\text{HVP,LO}} = a_\mu^{\text{SD}} + a_\mu^{\text{W}} + a_\mu^{\text{LD}}$ . Their time-momentum representations of (2.5) are given as

$$\begin{aligned} a_\mu^{\text{SD}} &= 4\alpha^2 m_\mu \int_0^{\tau_c} d\tau [1 - \Theta(\tau, \tau_0; \Delta)] \tau^3 G(\tau) \tilde{K}_E(\tau), \\ a_\mu^{\text{W}} &= 4\alpha^2 m_\mu \int_0^{\tau_c} d\tau [\Theta(\tau, \tau_0; \Delta) - \Theta(\tau, \tau_1; \Delta)] \tau^3 G(\tau) \tilde{K}_E(\tau), \\ a_\mu^{\text{LD}} &= 4\alpha^2 m_\mu \int_0^{\tau_c} d\tau \Theta(\tau, \tau_1; \Delta) \tau^3 G(\tau) \tilde{K}_E(\tau). \end{aligned} \quad (5.2)$$

The separation points are set as  $\tau_0 = 0.4$  fm and  $\tau_1 = 1.0$  fm, and the width  $\Delta$  of the smearing is set to 0.15 fm. We take  $\tau_c = 10$  fm, which nearly saturate the integral up to  $\infty$ .

Similarly to Figures 14 and 15, we plot the estimates of the finite-volume effect for each time window in Figure 17 (versus  $m_\pi L$ ) and in Figure 18 (versus  $1/(m_\pi L)^2$ ). Different



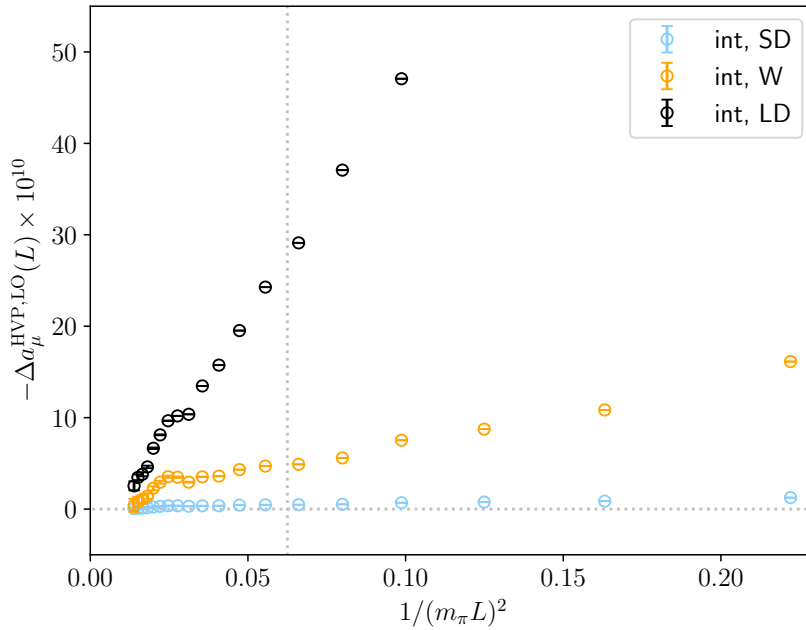


**Figure 18.** Finite-volume effect for  $a_\mu^{\text{HVP,LO}}$  evaluated for different Euclidean time windows, plotted as a function of  $1/(m_\pi L)^2$ . The error bar is from the extrapolation in the energy cutoff  $E_{\pi\pi,\text{cut}}$  (see Section 4.3).

windows are distinguished by different colors. The finite-volume effect is most significant for the long-distance (LD) window, and its dependence on  $m_\pi L$  is very similar to those of sharp-cut windows.

The numerical values are listed in Table 1. The errors are from the extrapolation in the energy cut-off  $E_{\pi\pi,\text{cut}}$  (see Section 4.3). Other sources of errors, such as those from the input parameters as well as from the ignored inelastic states, are not shown.

## 6 Conclusion

In this paper, the finite-volume effect for the contribution of leading-order hadronic vacuum polarization to the muon  $g - 2$ ,  $a_\mu^{\text{HVP,LO}}$ , is studied in detail using phenomenological inputs. Unlike previous works [3, 7, 8], we explicitly construct the Euclidean correlator in a box assuming that only two-pion states contribute without any truncation of the pion’s wrapping-around effect. The phenomenological inputs are the  $\pi\pi$  phase shift and the time-like pion form factor, both of which can be consistently parametrized using the Gounaris-Sakurai model.

The  $\pi\pi$  states in this analysis satisfy Lüscher’s quantization condition, and their energy spectrum automatically reflects the wrapping-around effect to all orders, in contrast to previous studies that include only the leading terms. The Euclidean correlator  $G(\tau, L)$  at a finite volume  $L$  thus constructed shows a different volume dependence for different Euclidean time separations  $\tau$ . Asymptotically, the infinite volume limit is approached as

$L$ [fm]	SD	W	LD	total
3.0	1.2	16.1	98.3	115.6
3.5	0.9	10.8	75.0	86.8
4.0	0.8	8.8	58.9	68.4
4.5	0.7	7.5	47.1	55.3
5.0	0.5	5.6	37.1	43.2
5.5	0.5	4.9	29.1	34.5
6.0	0.5	4.7	24.3	29.4
6.5	0.4	4.3	19.5	24.3
7.0	0.4	3.6	15.7	19.7
7.5	0.4	3.5	13.5	17.4(1)
8.0	0.3	2.0(1)	10.4	13.6(1)
8.5	0.4	3.5(1)	10.2	14.0(1)
9.0	0.4	3.5(1)	9.7	13.6(2)
9.5	0.3	2.9(2)	8.1(1)	11.4(2)
10.0	0.2(1)	2.3(2)	6.7(1)	9.2(4)
10.5	0.2(1)	1.4(3)	4.6(1)	6.2(5)
11.0	0.1(1)	1.1(4)	3.8(2)	5.0(7)
11.5	0.1(1)	0.8(5)	3.5(3)	4.4(1.0)
12.0	0.1(1)	0.4(7)	2.5(5)	3.3(1.3)
$\infty$	12.19	119.1	294.9	426.2

**Table 1.**  $-\Delta a_\mu^{\text{HVP,LO}} \times 10^{10}$  for three Euclidean time windows, short-distance (SD), intermediate (W) and long-distance (LD), as well as a sum over them corresponding to the total contribution. The errors are from the extrapolation in the energy cutoff  $E_{\pi\pi,\text{cut}}$  (see Section 4.3). If the error is not written, it is smaller than the last digit shown. The last line is  $a_\mu^{\text{HVP,LO}} \times 10^{10}$  in the infinite volume.

$\exp(-m_\pi L^2/4\tau)$ , while an approximate power scaling  $1/L^\alpha$  is expected in the intermediate volume region.

The hadronic vacuum polarization contribution to  $a_\mu$  is obtained by a weighted integral over Euclidean time dominated in the region around  $\tau \sim 1$  fm. The overall  $L$  dependence is then not simply described by a single functional form. It turns out that the finite-volume effect  $\Delta a_\mu^{\text{HVP,LO}}$  shows an approximately linear dependence on  $1/(m_\pi L)^2$  in the region  $1/(m_\pi L)^2 > 0.05$ , and rapidly decreases in the larger volume region. Their size is larger than the estimate reported by Hansen and Patella [8], most likely due to the resonance enhancement of the  $\rho$ -meson.

Our analysis fills the gap between the exponential finite-volume scaling based on *e.g.* chiral effective theory and the power-law dependence expected from Lüscher’s quantization condition. Such a complication may arise for other quantities, for which the lowest-lying part of the spectrum is given by two-body states, although it became most critical for  $a_\mu$  because of its high required precision.

Similar analysis can be done for heavier pions employed in many lattice calculations,

provided that the phase shift and pion form factor are available. In other words, these quantities will provide a means of estimating finite-volume effects in the lattice calculations of  $a_\mu$ . When the lattice data are available on multiple volumes, this analysis would provide a highly non-trivial cross-check, as it is based on rather solid ground at least for the finite-volume effects.

Finally we note that our analysis is not complete as it could not take account of the inelastic states, such as four pions, and the realistic estimate can be obtained only with the full scale simulations such as those of [1, 22, 26]. However, the most important contribution from the  $\pi\pi$  states would be well captured by our analysis.

## Acknowledgments

We thank Kohtaroh Miura for discussions. SH is partly supported by MEXT as “Program for Promoting Researches on the Supercomputer Fugaku” (JPMXP1020200105) and by JSPS KAKENHI, Grant-Number 22H00138.

## References

- [1] S. Borsanyi et al., *Leading hadronic contribution to the muon magnetic moment from lattice QCD*, *Nature* **593** (2021) 51 [[2002.12347](#)].
- [2] MUON G-2 collaboration, *Measurement of the Positive Muon Anomalous Magnetic Moment to 0.20 ppm*, *Phys. Rev. Lett.* **131** (2023) 161802 [[2308.06230](#)].
- [3] C. Aubin, T. Blum, P. Chau, M. Golterman, S. Peris and C. Tu, *Finite-volume effects in the muon anomalous magnetic moment on the lattice*, *Phys. Rev. D* **93** (2016) 054508 [[1512.07555](#)].
- [4] J. Bijnens and J. Releford, *Vector two-point functions in finite volume using partially quenched chiral perturbation theory at two loops*, *JHEP* **12** (2017) 114 [[1710.04479](#)].
- [5] C. Aubin, T. Blum, M. Golterman and S. Peris, *Application of effective field theory to finite-volume effects in  $a_\mu^{HVP}$* , *Phys. Rev. D* **102** (2020) 094511 [[2008.03809](#)].
- [6] C. Aubin, T. Blum, M. Golterman and S. Peris, *Muon anomalous magnetic moment with staggered fermions: Is the lattice spacing small enough?*, *Phys. Rev. D* **106** (2022) 054503 [[2204.12256](#)].
- [7] M.T. Hansen and A. Patella, *Finite-volume effects in  $(g-2)_\mu^{HVP,LO}$* , *Phys. Rev. Lett.* **123** (2019) 172001 [[1904.10010](#)].
- [8] M.T. Hansen and A. Patella, *Finite-volume and thermal effects in the leading-HVP contribution to muonic  $(g-2)$* , *JHEP* **10** (2020) 029 [[2004.03935](#)].
- [9] M. Lüscher, *Two particle states on a torus and their relation to the scattering matrix*, *Nucl. Phys. B* **354** (1991) 531.
- [10] L. Lellouch and M. Lüscher, *Weak transition matrix elements from finite volume correlation functions*, *Commun. Math. Phys.* **219** (2001) 31 [[hep-lat/0003023](#)].
- [11] C.J.D. Lin, G. Martinelli, C.T. Sachrajda and M. Testa,  *$K \rightarrow \pi\pi$  decays in a finite volume*, *Nucl. Phys. B* **619** (2001) 467 [[hep-lat/0104006](#)].

- [12] H.B. Meyer, *Lattice QCD and the Timelike Pion Form Factor*, *Phys. Rev. Lett.* **107** (2011) 072002 [[1105.1892](#)].
- [13] D. Bernecker and H.B. Meyer, *Vector Correlators in Lattice QCD: Methods and applications*, *Eur. Phys. J. A* **47** (2011) 148 [[1107.4388](#)].
- [14] G.J. Gounaris and J.J. Sakurai, *Finite width corrections to the vector meson dominance prediction for  $\rho \rightarrow e^+e^-$* , *Phys. Rev. Lett.* **21** (1968) 244.
- [15] A. Francis, B. Jaeger, H.B. Meyer and H. Wittig, *A new representation of the Adler function for lattice QCD*, *Phys. Rev. D* **88** (2013) 054502 [[1306.2532](#)].
- [16] X. Feng, S. Aoki, S. Hashimoto and T. Kaneko, *Timelike pion form factor in lattice QCD*, *Phys. Rev. D* **91** (2015) 054504 [[1412.6319](#)].
- [17] D. Giusti, F. Sanfilippo and S. Simula, *Light-quark contribution to the leading hadronic vacuum polarization term of the muon  $g-2$  from twisted-mass fermions*, *Phys. Rev. D* **98** (2018) 114504 [[1808.00887](#)].
- [18] M. Cè et al., *Window observable for the hadronic vacuum polarization contribution to the muon  $g-2$  from lattice QCD*, *Phys. Rev. D* **106** (2022) 114502 [[2206.06582](#)].
- [19] FERMILAB LATTICE, HPQCD, MILC collaboration, *Light-quark connected intermediate-window contributions to the muon  $g-2$  hadronic vacuum polarization from lattice QCD*, *Phys. Rev. D* **107** (2023) 114514 [[2301.08274](#)].
- [20] RBC, UKQCD collaboration, *Calculation of the hadronic vacuum polarization contribution to the muon anomalous magnetic moment*, *Phys. Rev. Lett.* **121** (2018) 022003 [[1801.07224](#)].
- [21] T. Aoyama et. al., *The anomalous magnetic moment of the muon in the Standard Model*, *Phys. Rept.* **887** (2020) 1 [[2006.04822](#)].
- [22] A. Boccaletti et al., *High precision calculation of the hadronic vacuum polarisation contribution to the muon anomaly*, [2407.10913](#).
- [23] C. Lehner and A.S. Meyer, *Consistency of hadronic vacuum polarization between lattice QCD and the  $R$ -ratio*, *Phys. Rev. D* **101** (2020) 074515 [[2003.04177](#)].
- [24] CHIQCD collaboration, *Muon  $g-2$  with overlap valence fermions*, *Phys. Rev. D* **107** (2023) 034513 [[2204.01280](#)].
- [25] RBC, UKQCD collaboration, *Update of Euclidean windows of the hadronic vacuum polarization*, *Phys. Rev. D* **108** (2023) 054507 [[2301.08696](#)].
- [26] T. Blum et al., *The long-distance window of the hadronic vacuum polarization for the muon  $g-2$* , [2410.20590](#).
- [27] T. Blum, *Lattice calculation of the lowest order hadronic contribution to the muon anomalous magnetic moment*, *Phys. Rev. Lett.* **91** (2003) 052001 [[hep-lat/0212018](#)].
- [28] X. Wang, *ASYMPTOTICS OF THE  $q$ -THETA FUNCTION*, *Communications in Mathematical Analysis* **7** (2009) 50.
- [29] M. Luscher, *Signatures of unstable particles in finite volume*, *Nucl. Phys. B* **364** (1991) 237.
- [30] V.M. Aul'chenko et al., *Measurement of the  $e^+e^- \rightarrow \pi^+\pi^-$  cross section with the CMD-2 detector in the 370 - 520-MeV c.m. energy range*, *JETP Lett.* **84** (2006) 413 [[hep-ex/0610016](#)].

- [31] CMD-2 collaboration, *High-statistics measurement of the pion form factor in the rho-meson energy range with the CMD-2 detector*, *Phys. Lett. B* **648** (2007) 28 [[hep-ex/0610021](#)].
- [32] M.N. Achasov et al., *Update of the  $e^+e^- \rightarrow \pi^+\pi^-$  cross-section measured by SND detector in the energy region  $400\text{-MeV} < s^{**}(1/2) < 1000\text{-MeV}$* , *J. Exp. Theor. Phys.* **103** (2006) 380 [[hep-ex/0605013](#)].
- [33] KLOE collaboration, *Measurement of  $\sigma(e^+e^- \rightarrow \pi^+\pi^-)$  from threshold to  $0.85\text{ GeV}^2$  using Initial State Radiation with the KLOE detector*, *Phys. Lett. B* **700** (2011) 102 [[1006.5313](#)].
- [34] BABAR collaboration, *Precise Measurement of the  $e^+e^- \rightarrow \pi^+\pi^-(\gamma)$  Cross Section with the Initial-State Radiation Method at BABAR*, *Phys. Rev. D* **86** (2012) 032013 [[1205.2228](#)].
- [35] G. Colangelo, M. Hoferichter and P. Stoffer, *Two-pion contribution to hadronic vacuum polarization*, *JHEP* **02** (2019) 006 [[1810.00007](#)].
- [36] G. Colangelo, M. Hoferichter, B. Kubis and P. Stoffer, *Isospin-breaking effects in the two-pion contribution to hadronic vacuum polarization*, *JHEP* **10** (2022) 032 [[2208.08993](#)].
- [37] P. Estabrooks and A.D. Martin,  *$\pi\pi$  Phase Shift Analysis Below the  $K$  anti- $K$  Threshold*, *Nucl. Phys. B* **79** (1974) 301.
- [38] S.D. Protopopescu, M. Alston-Garnjost, A. Barbaro-Galtieri, S.M. Flatte, J.H. Friedman, T.A. Lasinski et al.,  *$\pi\pi$  Partial Wave Analysis from Reactions  $\pi^+p \rightarrow \pi^+\pi^-\Delta^{++}$  and  $\pi^+p \rightarrow K^+K^-\Delta^{++}$  at  $7.1\text{-GeV}/c$* , *Phys. Rev. D* **7** (1973) 1279.
- [39] M. Davier, A. Hoecker, B. Malaescu and Z. Zhang, *A new evaluation of the hadronic vacuum polarisation contributions to the muon anomalous magnetic moment and to  $\alpha(\mathbf{m}_Z^2)$* , *Eur. Phys. J. C* **80** (2020) 241 [[1908.00921](#)].
- [40] A. Keshavarzi, D. Nomura and T. Teubner,  *$g - 2$  of charged leptons,  $\alpha(M_Z^2)$ , and the hyperfine splitting of muonium*, *Phys. Rev. D* **101** (2020) 014029 [[1911.00367](#)].